UNIVERSITÀ DEGLI STUDI DI NAPOLI FEDERICO II

NOVEL STRATEGY TO PRODUCE NON-SPHERICAL POLYMERIC MICROPARTICLES FOR DRUG DELIVERY AND TISSUE ENGINEERING

RELATORE
PROF. PAOLO ANTONIO NETTI

CORRELATORE
DR. ING. RAFFAELE VECCHIONE

COORDINATORE
PROF. GIUSEPPE MENSITIERI

CANDIDATO
ING. RENATO DE ALTERIIS

2012-2015

PREFACE

Current technologies to encapsulate labile molecules into polymeric particles have been optimized for effectively protect such molecules from inactivation occurring in biological environments and preserve their bioactivity during release up to several weeks. To date, this demanding task is only addressed by particles which are spherical in shape. Considering the expertise already available for spherical particle technology, the use of microspheres as starting material to produce particles with different shape in order to broaden the scenario of drug delivery and tissue engineering is particularly attractive. Nevertheless, currently used processing techniques, involving heating and excessive solvent quantities, might alter the properties of the starting microspheres, affecting the release and the biological activity of labile molecules. The aim of this study was to develop a general method to produce polymeric particles of non-spherical shape encapsulating labile biomolecules starting from spherical particles, suitable for applications in the field of drug delivery and tissue engineering.

This thesis is organized into:

a *general introduction*, where literature on the role of particle shape and the current methods to produce non-spherical particles are reported, and where it will be shown that while the technology already available for particles which are spherical in shape has reached a certain level of maturity, the production processes of particles with different geometries still need further improvements;

a *main section*, where the most relevant results are described. This section along with the following experimental section is self-standing;

an *experimental section*, where materials and methods are described. This section also includes some scientific background, which is relevant for a better understanding both of the solvent/non-solvent plasticization and of the quartz crystal microbalance which have been used herein;

a *supplementary section*, where some implementations and a variant of the new method are described;

an *appendix*, where part of the positive search report drafted by the European Patent Office concerning the international patent application on the proposed method is reported.

INDEX

ABSTRACT

The aim of this study was to develop a general method to produce polymeric particles of non-spherical shape and encapsulating labile biomolecules starting from previously fabricated spherical particles, suitable for applications in the field of drug delivery and tissue engineering. The main concern was not only to preserve the biological activity of such molecules during the production process, but also to provide elaborate particles which could release bioactive moieties over a long time span. To date, this demanding task is only addressed by particles which are spherical in shape. For instance, current protein encapsulation technologies of polymeric microspheres have been optimized for effectively protect their "protein cargo" from inactivation occurring in biological environments, preserving its bioactivity during release up to several weeks. Nevertheless, the scenario of drug delivery and tissue engineering would be greatly expanded by strategies that enable the production of particles both with complex shape and with the beneficial properties of spherical particles.

Therefore, as a proof of principle, it is has been developed an easy and effective stamp-based method to produce poly-lactic-glycolic-acid (PLGA) microparticles encapsulating Vascular Endothelial Growth Factor (VEGF), with different shapes. It has been demonstrated that PLGA microspheres can be deformed at room temperature exploiting solvent/non-solvent plasticization. To predict the depression of the glass transition temperature of the polymer due to solvent sorption, a thermodynamic model and measurements with a quartz crystal microbalance were employed.

Since the properties of the starting microspheres are not altered by the process conditions, this gentle method allows to produce shaped particles which provide a prolonged release of VEGF in active form, as verified by an angiogenic assay.

The retention of the biological activity of an extremely labile molecule, i.e. VEGF, let us to hypothesize that a wide variety of drugs and proteins encapsulated in thermoplastic polymers can be processed with this method.

It was also demonstrated that this method allows to produce shaped and porous microparticles made of gelatin, which are of great interest in the field of tissue engineering. Furthermore, needle-shaped microparticles for transdermal drug delivery, and sintered microparticles have been produced.

Graphical abstract
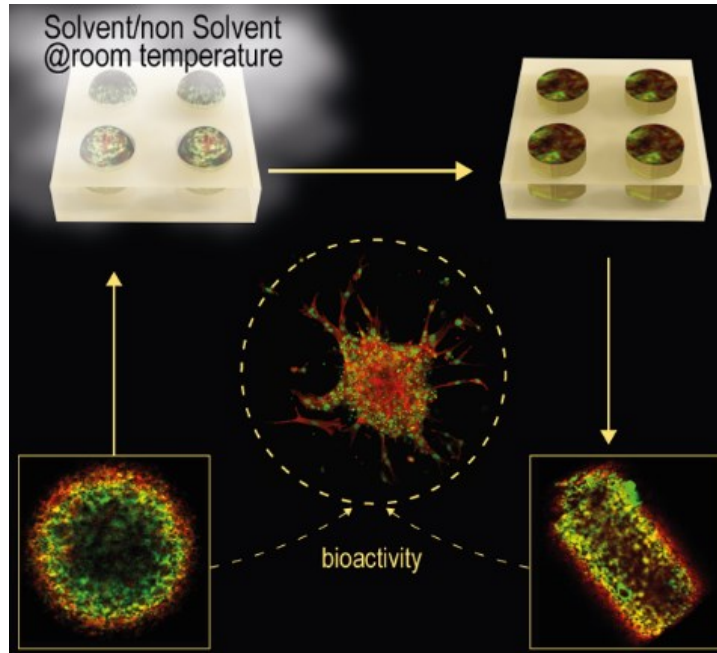
GENERAL INTRODUCTION

The role of particle shape in drug delivery and tissue engineering

Drug Delivery

It is nowadays recognized that shape is a useful tool in the toolbox for effective drug delivery particle design. Despite the precise role of particle shape in drug delivery has not been fully elucidated, certainly, shape, along with size, microstructure, surface chemistry and mechanical properties, is a critical feature which affects many *in vivo* performances, such as drug release profiles, bioadhesion, transport, targeting, and internalization.

Drug Release

Drug release of polymeric particles, as well as their degradation, is influenced by their size and shape.[1–3] When dealing with spherical particles, size is simply identified by sphere diameter. However, for non-spherical particles, size identification must be redefined since they may have two or more different length scales. For instance, one length scale may dominate the others and thus be a critical dimension. Therefore, non-spherical particles that have areas of different thicknesses could offer unique degradation profiles as the shape of the particle will change over time. Furthermore, drug release profiles can be affected by the higher surface area available for release as compared to spherical particles. It is worth mentioning that drug release is also affected by other features, such as porosity[4] and the material the particles are made of. For instance, for PLGA microparticles, the ratio of lactide to glycolide is a critical parameter.[5]

Bioadhesion

Particle shape may also affect bioadhesion on biosurfaces, such as walls of the buccal cavity, esophagus, gastrointestinal tract, genital tract, and blood vessels.[6] In particular, bioadhesion can be enhanced by using particles which, besides their cross sectional shape, have a flattened, or plate-like, geometry. This type of micro-particles has more surface-to-volume ratio than microspheres, and the area available for bioadhesion is much larger than that of microspheres. Moreover, if attached to a biosurface, a plate-

like microstructure would have smaller side area subject to the detaching force exerted by liquid flow and mechanical abrasion than a microsphere with the same volume. As a result, plate-like microparticles may have stronger and longer adhesion on biosurfaces.

Transport

Transport of particles in the body, regardless of the mode of administration, is also affected by particle shape, with particular reference to properties like particle velocity, diffusion and adhesion to walls in blood vessels, airways and intestine.[1]

For example, since non-spherical particles may align or tumble in the presence of flow, this behavior could have effects when particles flow through the tortuous pathways of filtering organs, such as the liver or spleen or when bifurcations in the vessels are encountered.

Internalization and targeting

Internalization of targeted particles, whether intended or undesired, could also be dictated by particle shape. Indeed, particle shape could affect the cells' ability not only to internalize successfully, but also the transport and sorting of the particle once inside the cell.[1,7]

Interestngly, it was compared targeted accumulation in tissues of spheres of various diameters (ranging from 100 nm to 10 μm) and elliptical discs of microscale dimensions (1 × 3 μm); it was found that targeting efficiency of micrometre-scale discs is better than any sphere, even those of nanometric dimensions.[8]

Another aspect concerns phagocytosis or in other words, the internalization of particles by macrophages, which is of interest since it prevents delivery of drugs to required tissues and is one of the primary obstacles of particulate drug delivery.

There is experimental evidence that phagocytosis by macrophages strongly depends on shape.[9] In fact, the local geometry of the particle can dictate whether macrophages initiate internalization. For example, with reference to Figure L1 ("L" is used for figures retrieved from the literature), a macrophage attached to an ellipse at the pointed end internalized it in a few minutes (Figure L1, a) while a macrophage attached to a flat region of the same ellipse did not internalize the particle for over 12 h (Figure L1, b). Spherical particles were internalized from any point of attachment, due to their symmetry (Figure L1, c).
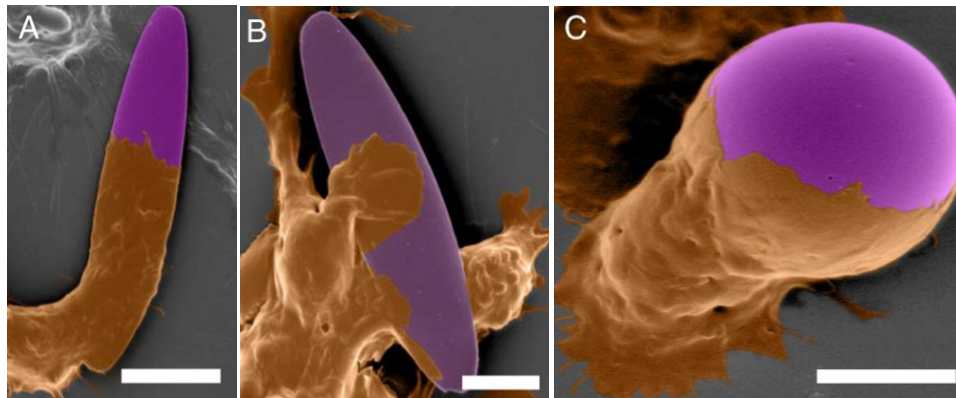
Figure L1. Effects of shape on phagocytosis. Scale bars 5 µm

Microneedles for transdermal drug delivery

One particular geometry to confer to polymer particles is that of micron-scale needles, or microneedles, which can be used for transdermal vaccination and drug delivery.

The use of microneedles for drug delivery was proposed in the 1970s and the first work on use of microneedles for transdermal drug delivery was reported in the late 1990s. While earlier designs provided microneedles made out of silicon, currently the use of metal and polymer microneedles has been emphasized. Microneedles can be employed in different ways, such as to pierce the skin to make it more permeable, or for injections in the case of hollow microneedles; furthermore, it is particularly attractive to use polymer microneedles which embed a therapeutic agent (Figure L2), in order to provide rapid or controlled release into the skin.

Materials employed for the production of this type of microneedles include poly-lactic-glycolic-acid (PLGA), carboxymethyl-cellulose, and poly-vinyl-pyrrolidone (PVP).[10]
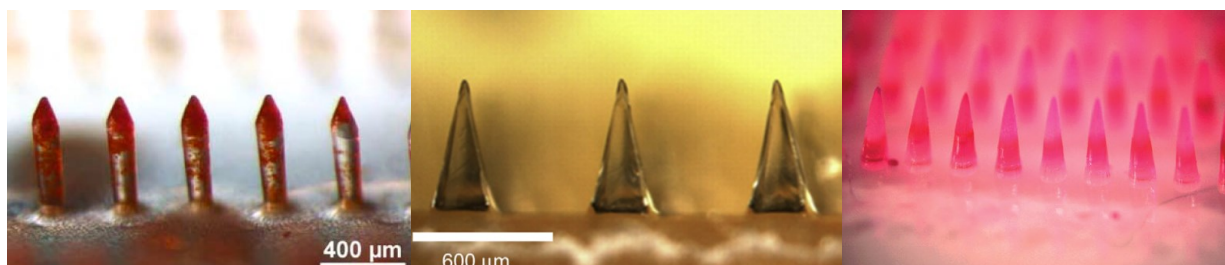

Figure L2. Microneedles made of poly-lactic-glycolic-acid (left), carboxymethyl-cellulose (center) poly-vinyl-pyrrolidone (right)

Transdermal drug delivery[11–13] by means of microneedles, which can be assembled as microneedles patches, is an effective alternative to conventional administration routes, such as oral delivery and hypodermic injection. Indeed, they can address the limitations associated with such conventional routes, such as biomolecule degradation, poor absorption in the gastrointestinal tract, pain, need of trained personnel and risk of infection. For instance, microneedles patches have been effectively used for influenza vaccination.[14,15]

Requirements for microneedles include the capability of inserting into skin without breaking, and of crossing the outermost layer of skin, i.e. a 10-20 μm thick layer called stratum corneum, which is the main barrier to transdermal drug delivery along with its 50-100 μm thick underlying layer, i.e. the viable epidermis, as recently reported.[16]

Typical microneedle geometries vary from 150 to 1500 μm in length, 50 to 250 μm in base width and 1 to 25 μm in tip diameter.

Polymer microneedles are widely produced with stamp based methods[12,17–20]; however, a mould-free fabrication technique which involves the electro-drawing of a polymer solution has also been proposed (Figure L3).[21]
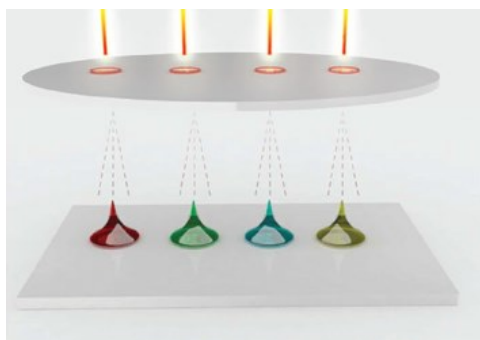

Figure L3. Electro-drawing of microneedles

Tissue Engineering

To enhance the function of engineered tissues there is a need to generate structures that mimic the intricate architecture and complexity of native organs and tissues.[22]

The classical "top-down" tissue engineering approach is based on the concept of seeding cells into preformed, porous, and biodegradable polymeric scaffolds that act as a temporary template for new tissue growth and reorganization. Nevertheless, one of the main limitation of this approach resides in the difficulty in recreating the architecture of native tissues.

By studying the nature of living tissues, it is possible to observe that most of them are composed of repeating units on the scale of hundreds of microns, with well-defined 3D microarchitectures and tissue-specific functional properties.[23] Examples, of such repeated functional units are the lobules in the liver, nephrons in the kidney, and muscle fibers. These "tissue modules" encompass the bulk of the function of the organs and tissues they comprise.

In light of this observation and to overcome the limitation of top-down approach, tissue engineering techniques are beginning to focus on building modular microtissues with repeated functional units. This emerging field known as modular tissue engineering focuses on fabricating tissue building blocks with specific microarchitectural features and assembling these modular units to engineer biological tissues, whereby this approach is usually called "bottom up".

In particular, modular tissue engineering aims to address the challenge of recreating biomimetic structures by designing structural features on the microscale to build modular tissues that can be used as building blocks to create larger tissues. Figure L4 shows the bottom-up and top-down approach.
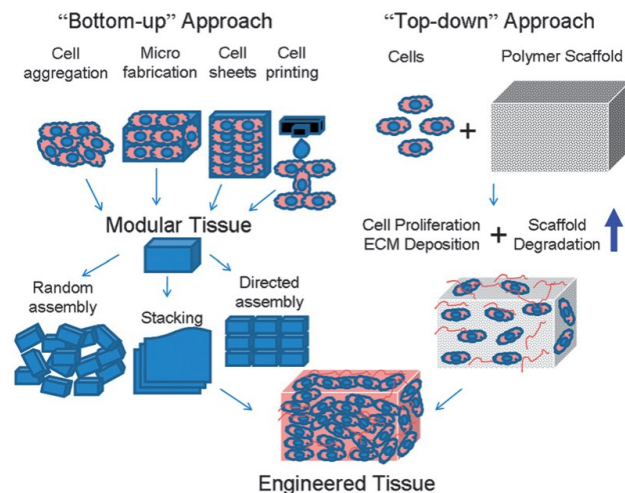

Figure L4. Bottom-up and Top-down approach

Given the ability to encapsulate cells in microscale gels, micro-fabrication techniques can be used to accurately recreate engineered tissue components of specific shapes and microarchitecture, as well as to assemble these structures into macroscale tissues, possibly after the assembly of primary structures into secondary and tertiary structures.

For example, microscale hydrogel blocks were fabricated in specific geometries to favor particular assembled secondary structures. It was also demonstrated that the secondary structures formed depend on the shape and aspect ratio of the rectangular microgel units. The concept of directed assembly was further demonstrated by creating complementary hydrogel structures, which naturally fit together in a lock-and-key mechanism. Hydrogels are widely used in tissue engineering since they closely resemble the native tissue matrix due to their high water content and polymeric network structure;[24–26] furthermore cell-laden hydrogels enable the confinement of different cells or materials to certain compartments in 3D structures.[27] This property can be used to control cell behavior in a spatially regulated manner.[28]

This showed that through careful design of the microgels, secondary and even tertiary structures could be predictably controlled. [28–30]

Porous gelatin hydrogel microspheres have also been used to create a 3D dermis[31] and cardiac muscle[23] equivalent *in vitro*. Gelatin, or denatured collagen, is an inexpensive material, which can be isolated from various animal sources relatively easily. Although it is denatured, it is a useful material since it maintains cell binding capacity.

Considering the importance of the role of particle shape to mimic the structure of target organs, and that of particle porosity to accommodate cells and maintain their viability, there is an increasing demand to expand the number of techniques available for the production of porous microparticles with specific geometries. Ideally, since tissue engineering is a highly multidisciplinary field, such microfabrication techniques should be affordable and easy to use.

Current methods to produce non-spherical microparticles

To date, considerable efforts have been made on the development of techniques providing non-spherical microparticles and many have been implemented.

Such methods have been classified as *ab initio*, as opposed to the manipulation of previously fabricated spherical particles into non-spherical geometries, i.e. *a posteriori*. *Ab initio* methods can be further classified, depending if they employ a microfluidic or stamp-based technology.

Microfluidic approaches[32–34], generally involve the formation of non-spherical microparticles within a microchannel and subsequent photopolymerization thereof. In particular, some recent stop flow lithography techniques have been able to provide highly monodisperse microparticles having complex shapes. The latter exploit the non-uniformity of the photopolymerizing UV light along the light path to create highly curved 3D particles.[33]

Referring now to the stamp-based techniques, they typically use a polymer solution or polymer melt as starting material to fill the cavities of a mold having the desired shape (Figure L5). Their development is also due to the wide number of shapes made available by the processes implemented in the recent years for the production of patterned substrates, such as photo-patterning.[35]
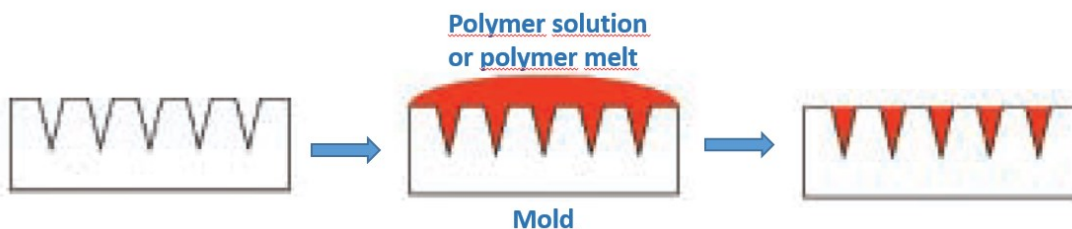

Figure L5. Scheme of a typical stamp based technique. A polymer solution or melt is used as starting material to produce shaped microparticles

Typically, such methods are based on a technology known as "soft lithography"[35–37], which encompasses a broad suite of processes for fabricating micro- and nano-scale features, by means of elastomeric stamps. In order to produce such stamps, a substrate which is patterned with the desired features is firstly produced, for example with a photo-lithographic technique. Subsequently, a material in liquid form, typically an uncured polymer resin, is poured onto the master and allowed to cure. After curing, the newly shaped solid material is separated from the master. The resulting stamp will have negative features with respect to the master. For example, when a master with protruding features is

employed, a stamp with corresponding cavities will result.

Polydimethylsiloxane (PDMS) is one of the most used materials for elastomeric stamp production due to its large number of advantageous properties. Indeed, it is non-toxic, low-adhesive, optically transparent and chemically stable in a wide range of environments.

Stamps made of such material have been used for the production of particles with different shapes, including needle-shaped particles with relatively high aspect ratio.[38,39]

Stamps made of hydrogels, which are water soluble materials, have also been proposed to collect the formed particles by simply dissolving the templates.[3]

An issue related to stamp-based methods is the formation of a residual interconnecting film between molded particles. Therefore, the so called pattern replication in non-wetting templates[40] has used highly low-adhesive molds made of perfluoropolyether[41] to produce isolated, rather than layer-interconnected, particles (Figure L6).
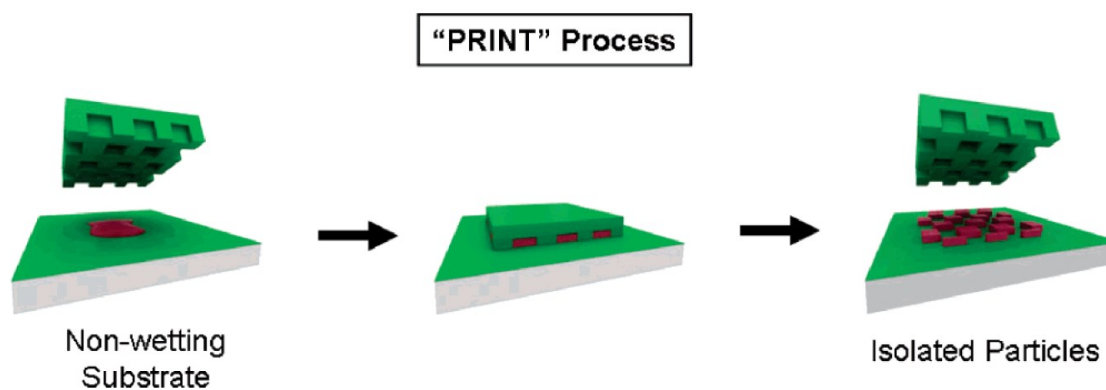

Figure L6. Schematic representation of the PRINT process

According to a variant of this method, stretching of the mold is employed in order to augment the variety of producible shapes.[42]

Ab initio methods can produce a broad range of shapes, but generally require a quite complex technology, and involve the use of harsh process conditions, e.g. high temperatures, and of harmful photoinitiators;[43] furthermore, the use of a polymer solution or melt as starting material does not allow to provide a high control on the internal microstructure and molecule distribution within microparticles.

A completely different approach has been proposed by Mitragotri et al.,[44] wherein previously produced spherical particles are deformed into different shapes. In particular, microparticles with a wide variety of shapes can be obtained liquefying microspheres, by means of heating or immersion in solvent, and

stretching of the polymer matrix. The shape of such particles basically depends on the liquefaction method and on the stretching directions. As shown in Figure L7, according to this method, stretching of the polymer matrix can be performed after (scheme A) or before (scheme B) liquefaction. In his first study, Mitragotri et al. reported the deformation of microspheres made of polystyrene, achieving liquefaction at 120 °C or by immersion in toluene. Again, the use of such high temperatures or excessive solvent quantities represent a limitation of this technique, in particular when dealing with labile molecules and when attempting to achieve porous microparticles with specific molecule distribution.
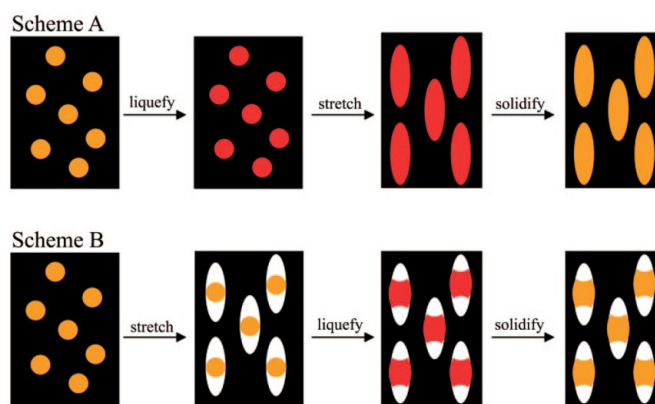

Figure L7. Method proposed by Mitragotri et. al.

Spherical and non-spherical microparticles for delivery of labile molecules

Delivery of extremely labile molecules, such as growth factors, is a demanding task. It will be shown that while the technology already available for particles which are spherical in shape has reached a certain level of maturity, the production processes of non-spherical particles still need further improvements.

A growth factor is a naturally occurring substance capable of stimulating cellular growth, proliferation, healing and cellular differentiation. Usually it is a protein or a steroid hormone. The local presence of growth factors in a damaged or diseased tissue is crucial to regenerate its structure or function. However, the appropriate mode for making these factors available at the desired site remains unclear. Despite bolus delivery of these molecules is technically simple, it is not effective. Indeed, the subsequent distribution of the factors throughout the body and their rapid degradation may lead to undesirable systemic effects and toxicity, and an insufficient local concentration for the required time frame, respectively. In particular, intravenous injection is a delivery method which is not localized to the target tissue and is also ineffective because of the growth factors' short half-lives. Although very small quantities (picograms to nanograms) of growth factor are necessary to generate a cellular response, growth factors are rapidly degraded. The biologic half-lives of platelet-derived growth factor (PDGF), basic fibroblast growth factor (bFGF or FGF-2), and vascular endothelial growth factor (VEGF), for example are 2, 3, and 50 min respectively, when intravenously injected. Direct therapeutic application of growth factors therefore requires substantial systemic doses at levels that can generate undesired effects.

These issues have motivated the development of controlled delivery systems that allow the sustained and localized delivery of small amounts of these factors to the target cell population and tissue site.

Such delivery also meets the requirement of providing a prolonged release, e.g. up to months, of growth factors in active form. Indeed, since the encapsulation of a growth factor in a polymeric material is typically involved, these systems protect their cargo from degradation in biological environment, and release just small amounts of active molecule over time, during the tissue growth.

Nevertheless, this is often challenging to achieve because processes used to formulate protein delivery constructs may denature or deactivate protein. Therefore, methods of fabrication that do not require harsh solvents or high temperatures are often desirable.[45] Encapsulation of therapeutic agents in

polymeric microspheres has been proven to be effective and can be achieved with the well established technique of encapsulation by solvent evaporation.[46,47]

A successful example of delivery of VEGF, was achieved by encapsulating such molecule in polymeric microspheres made of PLGA[48,49]. Advantageously, their production process involved the co-encapsulation of BSA and Hp to stabilize VEGF during encapsulation and release, and a remarkable feature of such microspheres was the specific distribution of VEGF, BSA and HP within microspheres. Such microspheres were produced with a double emulsion-solvent evaporation technique. BSA, a surface active protein, was used as a "sacrificial lamb"[50] to compete with VEGF for interactions at water/oil interface, thus preventing VEGF aggregation during the emulsification process. Hp was used to stabilize VEGF by complexation; in particular, Hp, interacting with the specific binding domain, stabilizes the native structure of VEGF and promotes its interaction with receptors located at cell membranes. Interestingly, BSA surrounded Hp - and presumably VEGF as well, since it strongly interacts with Hp - thus providing a shield for the growth factor.

Remarkably, such microspheres allowed a sustained release of VEGF for more than 40 days at approximately constant rate of 0.6 ng/day per mg of microspheres.

On the other hand, few studies on the production of non-spherical microparticles have been specifically devoted to encapsulation of extremely labile molecules, and those available in the literature make use of *ab initio* methods.

For example, Prausnitz et al.[18] reported the production of microneedles made of poly (vinylpyrrolidone-co-methacrylic acid) and embedding β-galactosidase, a model protein. A liquid mixture of monomers and protein was used to fill the cavities of a PDMS mold and subsequently photo-polymerized *in situ*, i.e. with the mixture inside the mold. It was also demonstrated that β-galactosidase extracted from dissolved microneedles was active.

Furthermore, De Simone et. al.[40] used the pattern replication in non-wetting templates to produce conical-shaped poly ethylene glycol particles containing avidin, the biological activity of which was demonstrated by performing biotin-binding experiments. In particular, the bioactivity of avidin within microparticles was assessed by exposing the latter to a fluorescein-labeled biotin solution. Confocal microscope images revealed that avidin was co-localized with fluorescein-labeled biotin, which indicated the binding of biotin to the avidin-containing particles, and hence avidin bioactivity.

De Simone et al.[51] also proposed to directly mold neat insulin and albumin particles and that contain

therapeutic cargos including siRNA and paclitaxel. Since a protein is used to shield other molecules, this approach somehow departs from the more "traditional" and established methods of encapsulating proteins in polymeric materials, such as PLGA or PEG.

Nevertheless, the ability of shaped polymeric microparticles to deliver very labile biomolecules, such as growth factors, in their biological active form over time – which is to date possible by virtue of the encapsulation strategies developed for spherical particles – has not been proved yet.

Main Section

Introduction

Protein-encapsulated polymeric microspheres have been proved effective in releasing even very labile bioactive moieties in a specific manner at pre-programmed rates[45,52,53]. These systems effectively protect their "protein cargo" from inactivation occurring in biological environments and preserve its bioactivity during the release process[54]. For instance, Vascular Endothelial Growth Factor (VEGF), a potent angiogenic molecule, has to be properly encapsulated to allow its effective release over time, since it is extremely sensitive to environmental inactivation and is otherwise non-usable. Indeed, poly-lactic-glycolic-acid (PLGA) microspheres with elaborate architecture and formulation, loaded with VEGF complexed with heparin (Hp) and provided with a protective layer of bovine serum albumin (BSA), prolong VEGF half-life allowing its release in active form up to several weeks[49,48]. In addition, protein release profiles can be engineered by tuning microsphere size and microstructure with well-established protocols[4,47,55].

Although current protein encapsulation technologies have been optimized for the production of microspheres, the scenario of protein delivery would be greatly expanded by strategies that enable the production of particles with shapes more complex than merely spherical. Indeed, there is a growing body of evidence supporting the importance of the role of the shape of polymeric microparticles, especially in the fields of drug delivery and tissue engineering[7,56]. In terms of drug delivery, particle shape affects many *in vivo* performances, such as transport, targeting and internalization[1,57–59]. Furthermore, needle-shaped particles, i.e. microneedles, of hundreds of microns in size provide an effective tool for transdermal drug delivery[11,14,18]. In the field of tissue engineering, particle shape plays a key role in the so called bottom-up approach, wherein shaped microparticles mimic the microenvironment of specific tissues and are used as building blocks for their construction[22,31,60,61].

Various *ab initio* methods to produce microparticles with complex shapes have been described[1,33,34,40,51,62]. However, considering the expertise already available for spherical particle technology, the use of microspheres as a starting material to obtain microparticles with different shapes is more attractive. Mitragotri et al. proposed to deform previously fabricated microspheres embedded in a polymer matrix into non-spherical geometries[44]. In particular, microparticles with a wide

variety of shapes can be obtained liquefying microspheres, by means of heating or immersion in solvent, and stretching of the polymer matrix. However, the liquefaction of microspheres might affect the biological activity of labile embedded biomolecules and their effective release. In particular, this deformation method might alter the microstructure of the microspheres and the distribution of the protein cargo and its protective layer, thus jeopardizing the beneficial properties of the encapsulation strategies achieved for spherical particles.

Results

The new method

Driven by the willingness to better exploit the advantages related to the use of microspheres as a starting material, and considering the possible effects of liquefaction, the aim of this study was to develop a novel stamp-based technique to produce shaped and isolated microparticles by deforming previously fabricated microspheres under gentle process conditions (i.e. at room temperature by using a solvent/non-solvent vapor mixture) and to verify the release of VEGF in active form from the shaped microparticles over time.

Starting microspheres made of PLGA 50:50, with a porous internal microstructure and containing VEGF/Hp/BSA were produced with a double emulsion-solvent evaporation method, as previously reported[49,48]. In order to verify the molecule distribution within starting and deformed microspheres, fluorescent microspheres containing labeled probes, i.e. BSA-Alexa-647 and Hp-Rhod 6g, were obtained with the same procedure, and analyzed by confocal microscopy. In addition, microspheres loaded with Nile Red (NR) produced with a Micropore® system (see Experimental Section), were prepared to highlight the particle microstructure and analyzed by confocal microscope.

The amount of VEGF within the starting microspheres was quantified by a specific enzyme-linked immunosorbent assay (ELISA), while the proangiogenic activity of VEGF -as well as its effective release after deformation- were evaluated by *in vitro* sprouting angiogenesis assay.

It is known that an increase of macromolecule mobility is required to achieve plastic deformation. In the case of amorphous polymers like PLGA such deformation is typically obtained by heating them up to some tens of degrees above their glass transition temperature (Tg), which for commercial PLGA 50:50 is comprised between 46 and 50 °C. However, since many drug molecules are thermo-labile, such

relatively high temperatures should be avoided in order to retain the particle microstructure and biological activity of the embedded molecules.

In view of the above, we exploited the phenomenon of solvent plasticization, that is the depression of Tg due to sorption of small molecules -in particular solvent molecules- causing an increase in the mobility of macromolecules. This topic has stimulated an abundant literature; many thermodynamic models, chiefly based on the framework set by Gibbs and Di Marzio, have been proposed[63]. Among others, Chow et al.[64] proposed an explicit model for the prediction of the depression of Tg due to solvent sorption (see Experimental Section). Key parameters of the Chow model are the glass transition temperature of the pure polymer (Tg$_0$) and the change in specific heat (ΔCp) of the polymer associated with its glass transition temperature.

As a solvent, we selected dimethyl carbonate (DMC) because it is non-toxic. Since PLGA is rapidly dissolved by DMC, while ethanol (EtOH) is known to be a non-solvent for such polymer, a liquid mixture of DMC and EtOH was vaporized at room temperature onto microspheres located inside the mold cavities in order to achieve plasticization while avoiding dissolution. Working with solvent vapors instead of liquid solutions enabled us to enhance the gentleness of the process, in particular to keep the microstructure of the exposed microspheres.

In order to estimate the DMC mass fraction w in PLGA required for its plasticization, differential scanning calorimetry (DSC) measurements were performed, so that Tg$_0$ and ΔCp could be evaluated for the microspheres under study, and the Chow equation could be applied. DSC measurements were also carried out on stock PLGA; DSC thermograms revealed a Tg$_0$ of 48.87 °C, according to the manufacturer specification, while for the microspheres the Tg$_0$ was approximatively 10 °C lower, possibly due to a combination of several factors, such as the presence of other compounds, microstructure and process conditions (see Experimental Section, Figure 9). According to the Chow equation, the required range of DMC mass fraction w in the polymer required to lower the Tg$_0$ of the stock PLGA to room temperature was approximatively 0.1-0.14 (see Experimental Section, Figure 10).

Sorption of DMC by PLGA at room temperature was monitored via quartz crystal microbalance (QCM)[65,66], by successively exposing a thin polymer film to DMC/EtOH solutions with a constant increase of DMC mass fractions at each injection. Comparing the mass fraction of solvent in each solution with the corresponding solvent mass fraction within the polymer as evaluated by QCM (see

Experimental Section Fig. 18), and taking into account the Chow model, we could determine a narrow range of DMC to EtOH ratio within solution capable of effectively plasticize PLGA at room temperature. Furthermore, the increase in dissipation registered by the QCM instrument at such range (see Experimental Section, Fig. 16) gave a qualitative indication of the change of the elastic modulus of the polymer, which occurs when crossing its Tg.

Therefore, applying the Chow model to the microspheres to be deformed, we could similarly identify a narrow range of the DMC mass fraction within the solvent/non-solvent solution. The exposure time to plasticize microspheres at room temperature was experimentally determined at a fixed solvent mass fraction within the above range and fixed flow rate, i.e. about 0.145 and 20 μl/min.

As expected, we found that exposure time is dependent on microsphere porosity. Indeed, while 7 min were required to deform microspheres with a pore size of 2-5 μm, 1 min was sufficient for microspheres with a pore size of one order of magnitude larger. Such pore sizes corresponded to microspheres produced with the Micropore® system and the VEGF-loaded microspheres, respectively.

Figure 1 schematically shows the main steps of our shaping process. Briefly, PLGA microspheres loaded with NR or VEGF, with a diameter of about 200 μm, were placed inside the cavities of an elastomeric mold made of polydimethylsiloxane (PDMS), wherein each cavity had a volume similar to that of a microsphere. Next, microspheres were exposed to solvent vapors to achieve deformation at room temperature, and then demolded using a glass substrate and/or an adhesive tape. In this study, particles with three different shapes -namely, triangular prism, parallelepiped with a pyramid on top, and cylinder- were produced. In order to obtain the elastomeric stamps, each one consisting of an array of cavities with the desired size and shape, patterned master templates with corresponding protruding features were employed. In particular, master templates having cylindrical features were fabricated in-house by means of a micromilling machine. Stamps produced with such masters had cavities comprising a top portion having width equal to or larger than the microsphere diameter. This feature facilitated the filling of a lower portion of the cavities having the shape intended for the deformed microspheres, i.e. cylindrical shape with an aspect ratio of 1.25. VEGF loaded microspheres were deformed into such cylindrical shape. When the molding cavity has a width lower than the microsphere diameter, the deformation is aided by the elastic force exerted by the walls of the cavity, while when the microsphere

diameter is comparable with that of the molding cavity, deformation can be assisted by a flat substrate, such as a glass slide.
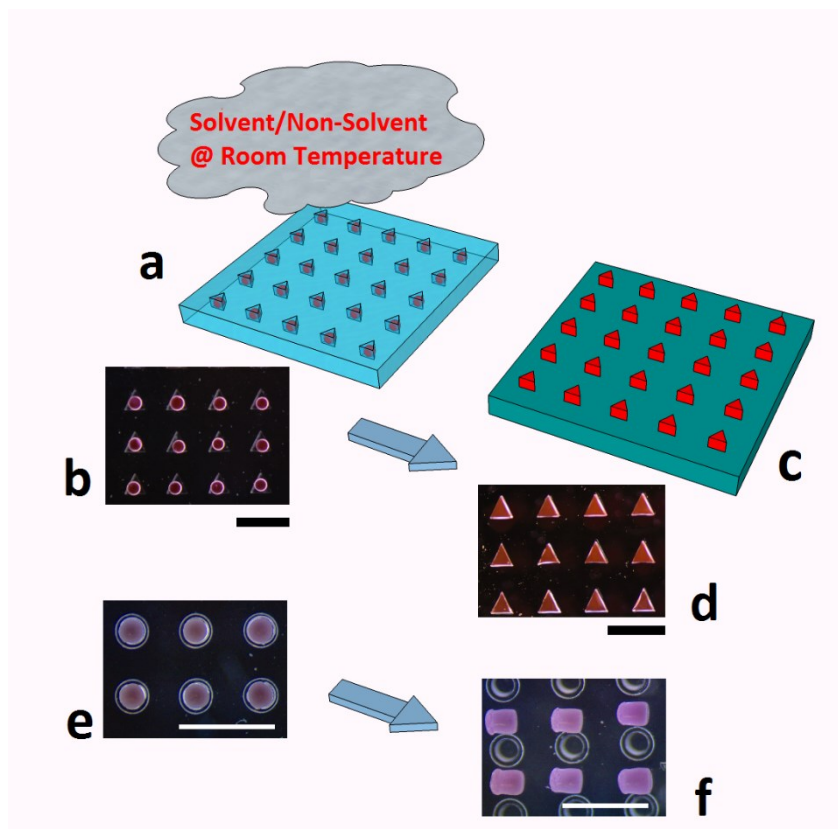

Figure 1. Fabrication of the shaped particles. a-b) PLGA microspheres loaded with NR, inside triangular prism-shaped cavities of a PDMS mold, exposed to a solvent/non-solvent (DMC/EtOH) vapor mixture at room temperature; c-d) Deformed microspheres released on a glass substrate; e) PLGA microspheres loaded with NR, inside cylindrical-shaped cavities having an enlarged top portion of a PDMS mold; f) Deformed microspheres extracted from the cylindrical-shaped cavities. PLGA, *polylacticglycolic acid*; NR, *nile red*; PDMS, *polydimethylsiloxane*; DMC, *dimethylcarbonate*; EtOH, *Ethanol*. Scale bars 750 μm

Particle characterization and molecule distribution.

After solvent evaporation, the shaped microparticles were inspected by a scanning electron microscope (SEM) which showed that deformation was achieved (Figure 2, a-d). In order to evaluate the internal microstructure, particles were cut with an ultra cryomicrotome and sections were SEM inspected (Figure 2, e, f; Figure 3, a, b); confocal microscope analysis of NR loaded microparticles (Figure 2, g, h) and micro-computed tomography (Figure 4) were also performed. In order to evaluate the distribution

of the molecules, confocal images of microparticles loaded with labeled BSA and Hp were obtained (Figure 2, i, j). As shown, the microstructure (Figure 2, e-h) and the distribution of BSA and Hp (Figure 2, i, j) of the shaped microparticles is very similar to that of the starting microspheres.
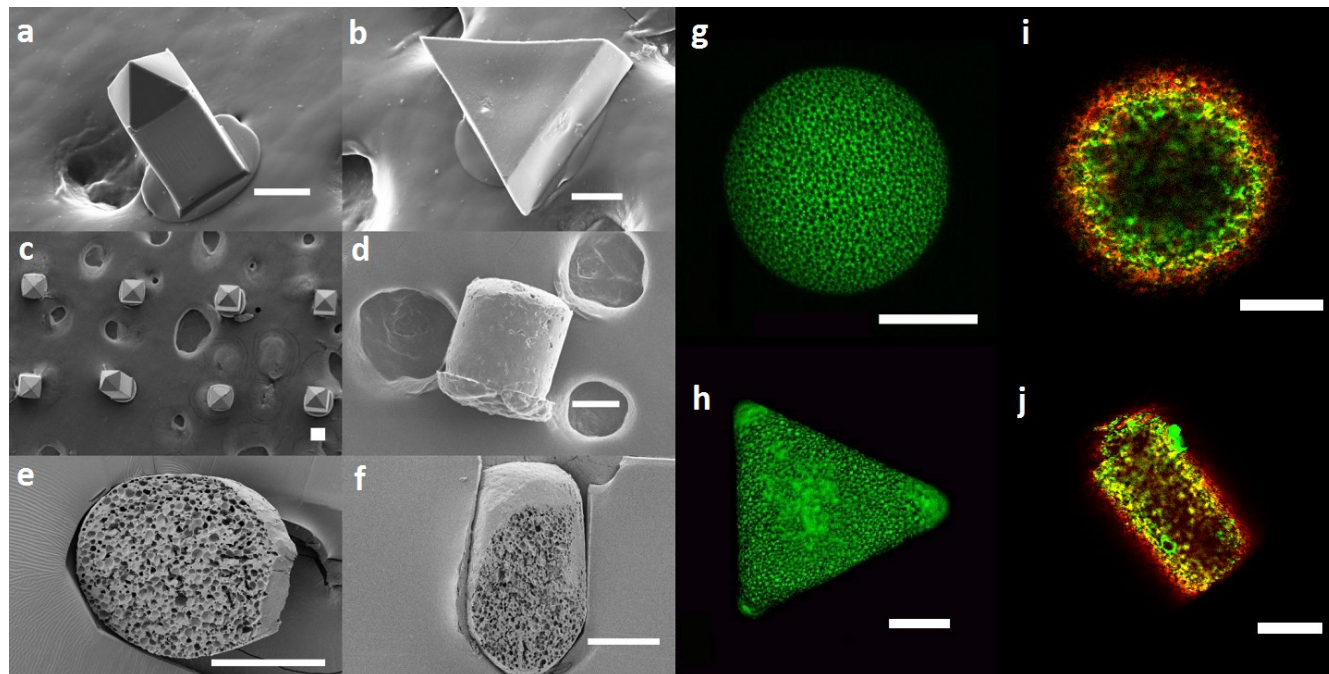

Figure 2. Particle morphology, microstructure and molecule distribution. SEM images of deformed microspheres loaded with NR (a-c), and of a deformed microsphere loaded with VEGF/Hp/BSA (d); SEM images of a sectioned microsphere (e), and of a sectioned deformed microsphere (f). Confocal microscope z-stack maximum projection of a microsphere (g), and of a deformed microsphere (h), both loaded with NR. Confocal microscope images of a microsphere (i) and of a deformed microsphere (j), both loaded with labeled BSA, red, and Hp, green. The microstructure (e-h) and the distribution of BSA and Hp (i, j) of the shaped microparticles is very similar to that of the starting microspheres. SEM, *Scanning electron microscope*, NR, *Nile Red*, VEGF, *Vascular Endothelial Growth Factor;* Hp, *heparin*, BSA, *bovine serum albumin*. Scale bars 75 μm
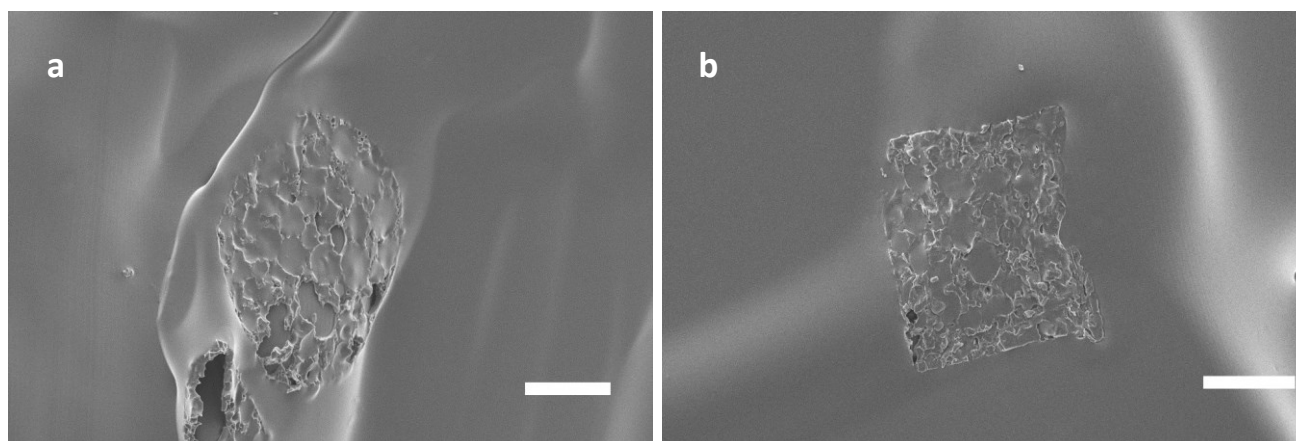

Figure 3. SEM images of a sectioned VEGF loaded microsphere (a), and of a sectioned deformed microsphere (b). The microstructure is very similar Scale bars 75 μm
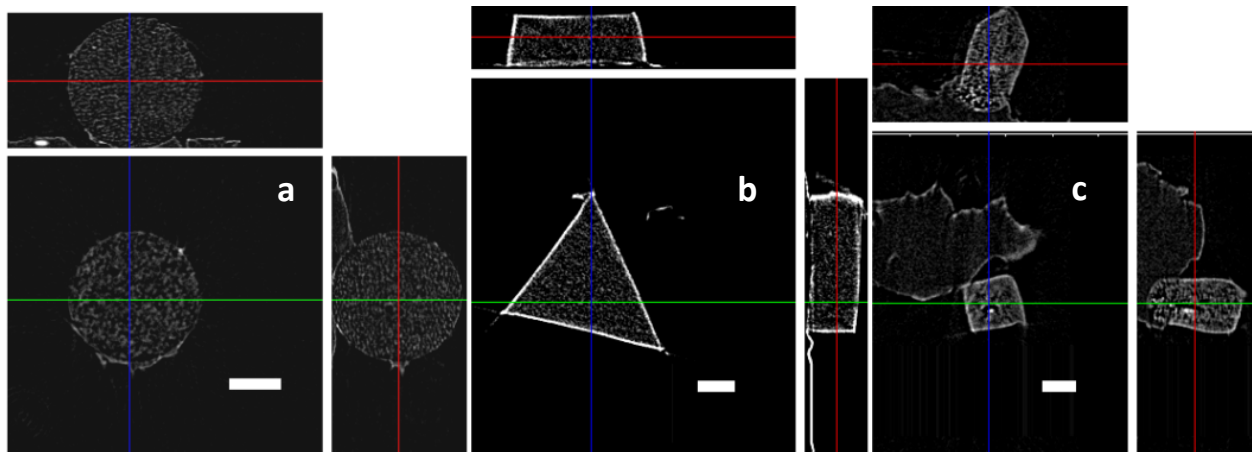
Figure 4. Micro computed tomography images of a NR loaded microsphere (a) and deformed microspheres (b, c). The microstructure is very similar. Scale bars 75 µm

VEGF release and bioactivity

The determination of the amount of the embedded VEGF by ELISA before and after deformation evidenced that the quantity of VEGF extracted from the deformed microspheres was equivalent to that extracted from the starting microspheres, i.e. about 50% (see Supplementary Information). However, as the retention of the VEGF activity was one of our main concerns, we further analyzed the VEGF activity before and after deformation by an *in vitro* sprouting angiogenesis assay, performed as previously reported[49]. Briefly, the proangiogenic activity of the VEGF content in the deformed microspheres (1 mg), as well as that encapsulated in 1 mg of starting microspheres, was evaluated on Human Umbilical Vein Endothelial Cells (HUVEC) and measured as sprout number and average sprout length. Results are summarized in Figure 5. Interestingly, at baseline (ET0), the proangiogenic activity of VEGF within the deformed microspheres was not statistically different from that of VEGF within the starting microspheres (Figure 5 a, b). Furthermore, in order to evaluate the release properties of VEGF from the deformed microspheres, which is strongly dependent on their internal microstructure, the activity of VEGF released from both starting and deformed microspheres was analyzed by carrying out a proangiogenic assay after incubation at 37 °C in 1 ml of cell culture medium for 7, 14, 21, and 30 days (RT7, RT14, RT21, and RT30, respectively). At each time, the activity of VEGF released in the cell culture medium was similar for both samples, when evaluated as sprout number (Figure 5, f). This finding denoted that both samples released comparable quantities of VEGF in the cell culture medium at each

time, thus confirming that deformed microspheres have a similar porosity to that of the starting microspheres. Interestingly, we observed a slight but significantly higher sprout length from deformed microspheres as compared to the starting microspheres, after 7 days (RT7, figure 5, g), possibly due to a higher release caused by the difference in shape. The remainder VEGF counterpart still entrapped within starting and deformed microspheres after incubation was also analyzed. In particular, samples showed a decreasing trend of the VEGF activity over time, thus confirming an effective VEGF release (Figure 6). As a comparison study, a further proangiogenic assay was carried out for microspheres deformed with the same plasticizing solution, but for different exposure times, i.e. 7 min and 1 min, and similarly incubated for 7 days (ET7). In this case, the activity of residual VEGF embedded in the deformed microspheres exposed for a longer time was higher than that embedded in the deformed microspheres exposed for a shorter time due to a lower release, denoting that an excessive plasticization leads to closure of the pores of the deformed microspheres (Figure 5 h, i).
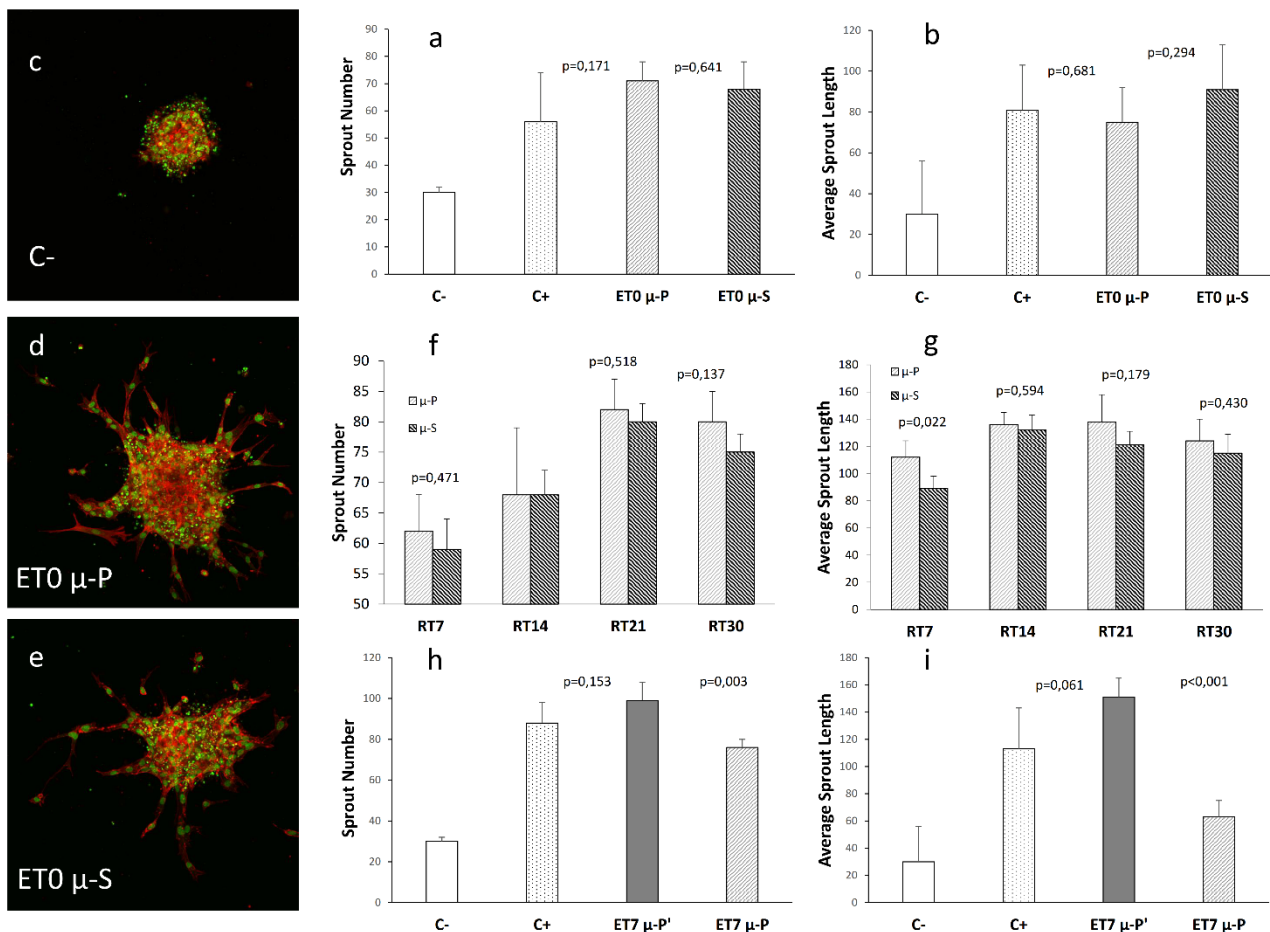

Figure 5. VEGF is released in active form over time. Proangiogenic activity of VEGF extracted or released from PLGA microspheres (μ-S) and deformed microspheres (μ-P), evaluated on HUVEC cells and measured as sprout number and

25

average sprout length (μm). (a-b): sprout number and average sprout length, respectively, of the VEGF extracted from μ-S and from μ-P at baseline (ET0). ET0 μ-P and ET0 μ-S present equal VEGF activity. Confocal images confirming a lower angiogenic response in C- (c), and the evidence of sprouting in both ET0 μ-P (d) and ET0 μ-S (e). (f-g): sprout number and average sprout length, respectively, of the VEGF released from μ-S and from μ-P, at 4 different time-points (RT7, RT14, RT21, RT30). When evaluating the sprout number, μ-S and μ-P present a similar VEGF activity at each time. When evaluating the sprout length, after 7 days of incubation (RT7) μ-P present a significantly higher VEGF activity. (h-i): sprout number and average sprout length, respectively, of the VEGF extracted from deformed microspheres after 7 days (ET7) of incubation, wherein μ-P' were deformed with a longer exposure time to solvent as compared to μ-P. ET7 μ-P' presents a higher residual VEGF activity, due to a lower release, as compared to that of ET7 μ-P. P values <0.05 were considered statistically significant. P values compared to C- were always < 0.01. C-, *negative control*; C+, *positive control*; VEGF, *Vascular Endothelial Growth Factor*; HUVEC*, Human Umbilical Vein Endothelial Cells;* PLGA, *poly-lactic-glycolic acid*.
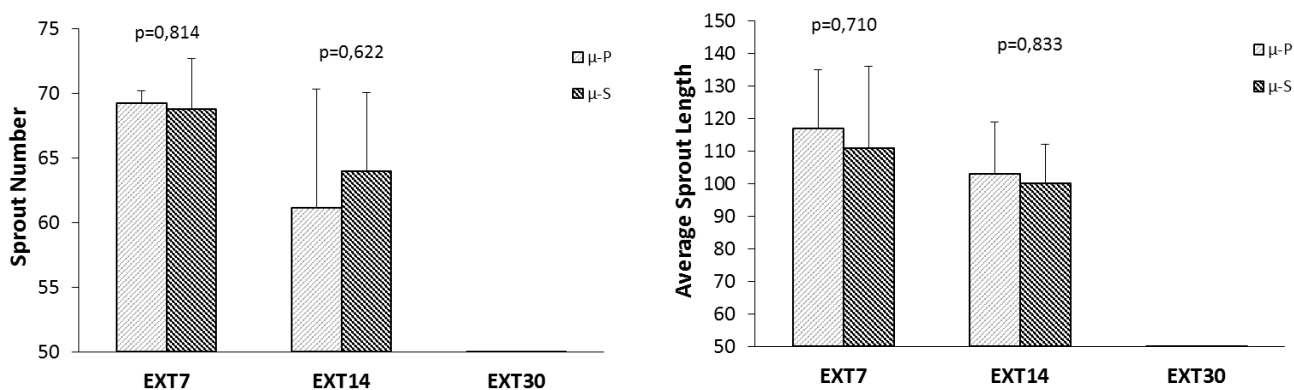

Figure 6. Activity of the remainder VEGF counterpart still entrapped in microspheres and deformed microspheres after incubation

Discussion

To sum up, we propose a new and effective method to produce non-spherical polymeric particles starting from previously fabricated PLGA microspheres loaded with VEGF/Hp/BSA, by exploiting solvent/non-solvent plasticization at room temperature using a vapor mixture. It is of our knowledge that some microfluidic[33,34], advanced non-wetting stamp based techniques[40,51], and particle reshaping methods[44,67] have been developed for the production of a broad size range of isolated, monodisperse, non-spherical microparticles. However, evidence that such microparticles can effectively release over time active form of labile proteins, such as VEGF, has not been provided so far.

Our method allows to preserve both the microstructure and molecule distribution of the starting microspheres, providing shaped microparticles that can release active VEGF over time. In particular, we demonstrate that the shaped microparticles keep a porous microstructure and VEGF/Hp/BSA distribution similar to that of the starting microspheres, whereby the release of the VEGF embedded in

26

the shaped microparticles and starting microspheres is equivalent. By contrast, we also demonstrate that an excessive plasticization leads to closure of the particle pores and, consequently, to a higher residual VEGF activity due to a lower release.

Remarkably, the retention of the biological activity of a very labile protein, such as VEGF, lets us hypothesize that a wide variety of different drugs and proteins can be processed with this method. In addition, the retention of the microstructure suggests the possibility to tune the drug release profiles from the shaped microparticles by selecting the desired porosity of the microspheres used as starting material. Another valuable aspect is that our deformation technique allows to effectively exploit particle formulation strategies and drug encapsulation methods already developed and available for microspheres.

Finally, beside PLGA, one of the most frequently used biomaterials for microsphere production and particularly suitable even for microneedles for transdermal drug delivery[17,21], other materials employed for drug delivery and tissue engineering are likely to be plasticized at room temperature exploiting Tg depression due to solvent sorption. To this regard, we performed preliminary tests on gelatin microspheres, produced as previously reported[31], which were deformed at room temperature employing water as a plasticizing solvent (see Supplementary Section).

Since the cylindrical microparticles present a higher surface area available for drug release as compared to the starting microspheres, a higher VEGF release would be expected. Although the sprout number due to the released VEGF is not significantly different between deformed and starting microspheres, it is of interest that the sprout elongation at 7 days of incubation is however higher for the deformed microspheres, presumably due to a non-monotonic mechanism of the sprouting propagation[68], The low aspect ratio of the cylinders employed and a degradation process may account for the lack of length difference for longer incubation times.

Although this aspect prompts further investigations to evaluate the effects of more elongated shapes on the release profiles of the embedded biomolecules, the strength of this study relies on the careful evaluation not only of the VEGF quantity entrapped within microparticles, but also on the effects of the processing conditions on the VEGF bioactivity, which supports the possible use of our process to produce shaped polymer microparticles preserving the effectiveness of the embedded labile biomolecules.

EXPERIMENTAL SECTION

VEGF-loaded microspheres production: Recombinant human VEGF was purchased from PeproTech EC Ltd (UK). VEGF/Hp (0.1 µg and 0.1 µg of Hp per mg of microspheres) loaded microspheres were produced by double emulsion-solvent evaporation technique. VEGF and Hp quantities were both 0.1 µg per mg of microspheres. BSA was used as an aid excipient (ratio VEGF/Hp/BSA 1:1:70 w/w/w). A VEGF/Hp/BSA solution in sterile PBS at pH 7.4 (500 µl) was poured into 2.5 ml of a PLGA solution in methylene chloride (10% w/v). The primary emulsion was generated by a high-speed homogenizer (Basic 25 equipped with a tool 6G, IKA, Germany) operating at 17,500 rpm for 1 min. Afterwards, the emulsion was added to 100 ml of 0.5% w/v aqueous PVA and stirred at 6000 rpm at room temperature (Heidolph, Germany) for 3 h to achieve solvent evaporation and subsequent microsphere hardening. Afterwards, microspheres were collected, washed 3 times with distilled water by centrifuge at 4 °C, 6000 rpm for 15 min (SL 16R, Thermo Scientific, Germany) and freeze-dried (Alpha 1-4 LSC, Christ) for 24 h (0.01 atm, -60 °C). Microspheres with a diameter ranging from 200 to 300 µm were obtained by sieving. Microspheres encapsulating labeled BSA-Alexa 647 and Hp-Rhod 6g were produced with a similar procedure.

VEGF-ELISA (Dosage of VEGF): In order to determine the amount of VEGF embedded within the starting and deformed microspheres, each sample was dissolved in 1 ml of methylene chloride and the entrapped VEGF was withdrawn with 1 ml of cell culture medium (M200). VEGF in solution with the culture medium was quantified by an enzyme-linked immunosorbent assay (ELISA) according to the manufacturer's procedures (development Kit 900-K10, PeproTech EC Ltd, UK). Briefly, 100 µl of VEGF standard solution or samples appropriately diluted were added to the wells of a microplate coated with a mouse monoclonal antibody against VEGF and incubated for 2 h at room temperature. The microplates were then washed 3 times with wash buffer. After complete removal of any remaining wash buffer, the detection antibody was added to each well and incubated for 2 h at room temperature. After washing, avidin-HRP conjugate was added to each well and incubated for 30 min at room temperature. Then, the microplates were washed and 100 µl ABTS were added to each well. Following color development, the optical density (OD) was measured at $\lambda = 405$ nm with wavelength correction set at 650 nm at 5 min intervals for approximately 30 min on a microplate reader (Varian Cary 100 Scan

UV/visible spectrophotometer, PelkinElmer). The linearity of the response was verified over VEGF concentration range 16–1000 pg ml–1 (r2 > 0.999). Results are expressed as encapsulation efficiency (ratio of actual to theoretical loading × 100) ± standard deviation of values collected from 3 different batches, which for the starting microspheres is 52.13 ± 3.29 and for the deformed microspheres is 45.28 ± 3.00.

Sample preparation for in vitro sprouting angiogenesis assay: The proangiogenic activity of VEGF embedded in starting and deformed microspheres, after the deformation process (ET0) and after incubation in cell culture medium at 37 °C for 7 days (ET7), was evaluated. In order to do this, two pairs of samples were prepared. Each pair consisted of 1 mg starting microspheres and 1 mg of deformed microspheres within a glass vial.

With reference to ET0, the starting and deformed microspheres were dissolved in 1 ml of methylene chloride and VEGF was withdrawn with 1 ml of cell culture medium (M200), which was used for the proangiogenic assay.
With reference to ET7, after careful removal of the supernatant, the same VEGF extraction procedure was used.

The proangiogenic activity of VEGF released from starting and deformed microspheres at different times was evaluated. The activity of the remainder VEGF counterpart still entrapped in microspheres and deformed microspheres was also analyzed. In order to do this, 3 pairs of samples were prepared. Each pair consisted of about 1 mg of starting microspheres and 1 mg of deformed microspheres within a glass vial. Vials were filled with 1 ml of cell culture medium (M200), and all samples were incubated ad 37 °C. At predetermined time-points, i.e. 7, 14, 21, and 30 days after incubation, the supernatant (400 µl) was withdrawn from each pair and frozen at -20 °C. The supernatant at 21 and 30 days was withdrawn from the same vial. The extraction of VEGF from microspheres and deformed microspheres after incubation was carried out as mentioned above. The supernatant and the extracted VEGF were used for the proangiogenic assay.

Cell culture and generation of endothelial spheroids: Human Umbilical Vein Endothelial Cells (HUVECs) (Lonza) were grown in Medium 200 supplemented with LSGS kit (Life-Technologies) at 37 °C

in 5% CO_2 and 100% relative humidity (RH). At early passages (II-IV) they were employed in order to generate endothelial spheroids.

After 3-4 days of culture, confluent HUVECs monolayers were trypsinized and 800 cells per spheroid were suspended in culture medium containing 0.25% (w/v) carboxymethylcellulose (Sigma), seeded into ultra-low-attachment round-bottom 96-well plates (Costar) and cultured as described to allow spheroids formation. After 24 h, spheroids were harvested, centrifuged at 900 rcf for 15 min, suspended in 1.2 mg/ml bovine skin collagen, transferred in 48-well plates (Falcon) and incubated. M 200 culture medium, supplemented with 2% FBS and 1% Pen Strep (10,000 U/ml penicillin G sodium, and 10,000 µg/ml streptomycin sulphate in 0.85% saline) (Gibco), was added once collagen had polymerized.

In vitro sprouting angiogenesis assay: Spheroids were divided into 4 groups of 8, and each group was used to test the bioactivity of VEGF (40 ng/ml) embedded in or released from microspheres and deformed microspheres. Groups were identified and treated as follows: positive control (VEGF 40 ng/ml), negative control (basal medium) and VEGF released and extracted from both microspheres and deformed microspheres. Positive controls were selected taking into account the encapsulation efficiency and previously reported data[48], showing that the activity of VEGF at baseline is about 85%. Spheroids were then incubated at 37 °C, 5% CO2, and 100% RH.

After a 18-24 h culture, gels were observed by an inverted light microscope before being fixed with 4% paraformaldehyde for at least 40 min, rinsed with PBS buffer and stained with Phalloidin tetramethylrhodamine B isothiocyanate (Sigma-Aldrich) and Sytox green (Invitrogen) for actin microfilaments and cellular nuclei respectively. Sprouting was evaluated by a Leica SP5 confocal laser scanning microscope using a HCX APO LU-V-l 10.0 X 0.30 water objective lens. Samples were excited with a 488 nm argon laser for nuclei detection, while for actin a 543nm He–Ne laser was employed. A 560–600 nm or a 505–530 nm emission was used to detect actin and nuclei, respectively. Images processing and quantitative analysis were performed by Leica LAS AF Version 2.7.3.9723 software.

NR-loaded microspheres production: NR-loaded microspheres were prepared by membrane emulsification followed by solvent evaporation. A Micropore® technologies equipment was employed. The primary emulsion was prepared adding 1 ml of DI water into 10 ml of a PLGA (Resomer RG 504H, Evonik, Germany) and Nile Red (0.1%, w/v) solution in methylene chloride (10%, w/v). W/O emulsion was generated by sonication (Branson 450, USA) setting the amplitude at 30% for 30 s This emulsion

was injected at 2 ml/min into the membrane equipment previously filled with 50 ml of a 1% polyvinyl alcohol (Mowiol 40-88, Sigma Aldrich) aqueous solution, where the rotational speed had been set to 276 rpm and the membrane was a hydrophilic membrane with pinhole diameters of 40 µm, and 200 µm pitch, to produce multiple emulsion W/O/W. Solvent evaporation and subsequent microsphere hardening were achieved by magnetic stirring (IKA, Germany) at room temperature. Afterwards, microspheres were collected, washed 3 times with distilled water by centrifuge at 4 °C, 6000 rpm for 15 min (SL 16R, Thermo Scientific, Germany) and freeze-dried (Alpha 1-4 LSC, Christ) for 24 h (0.01 atm, -60 °C).

Statistical analysis: Quantitative data are reported as mean values ± standard deviation (SD) of three independent experiments performed in duplicate. Differences between the experimental groups have been analyzed by one-way analysis of variance (ANOVA) and p values<0.05 were considered statistically significant.

Elastomeric stamps production: in order to produce different elastomeric stamps, 3 respective master templates were employed. The first was a Si/SU8 master, patterned with arrays of isosceles triangular prisms (L1= 260 µm, L2= 290 µm, H= 100 µm) while the second master was made of cyclo olefin polymer patterned with arrays of square base parallelepipeds with a pyramid on their top, i.e. micro-needles, (L=100 µm, H= 250 µm). Differently from the first two masters, the third was produced in-house by means of a micromilling machine (Minitech Machinery, US). An array of cylindrical cavities was obtained by drilling a polymetilmethacrilate substrate with a tip having a diameter of 200 µm for a depth of 300 µm. A second tip, having a diameter of 300 µm was employed, drilling for a depth of 50 µm onto the previously produced cylindrical reentrances, whereby cavities with an enlarged top portion were obtained. A heat curable Polydimethylsiloxane (Sylgard 184, Dow Corning), 10:1 (w/w), base : curing agent, was poured onto each master template and cured while in contact with the latter at 80 °C for 2 h. Since the PMMA master had reentrant features, we used a PDMS replica, which, after sylanization, in turn served as a master template for a second PDMS replica that had reentrant features, or cavities. Sylanization was achieved by exposing the first PDMS replica to oxygen plasma for 1 min, rapid immersion in a solution containing, in volume percent, 1% fluorolink, 1% acetic acid, 4% DI water and 94% isopropanol, and heating at 100 °C for 45 min.

A typical process to produce an elastomeric stamp is schematically shown in Figure 7.
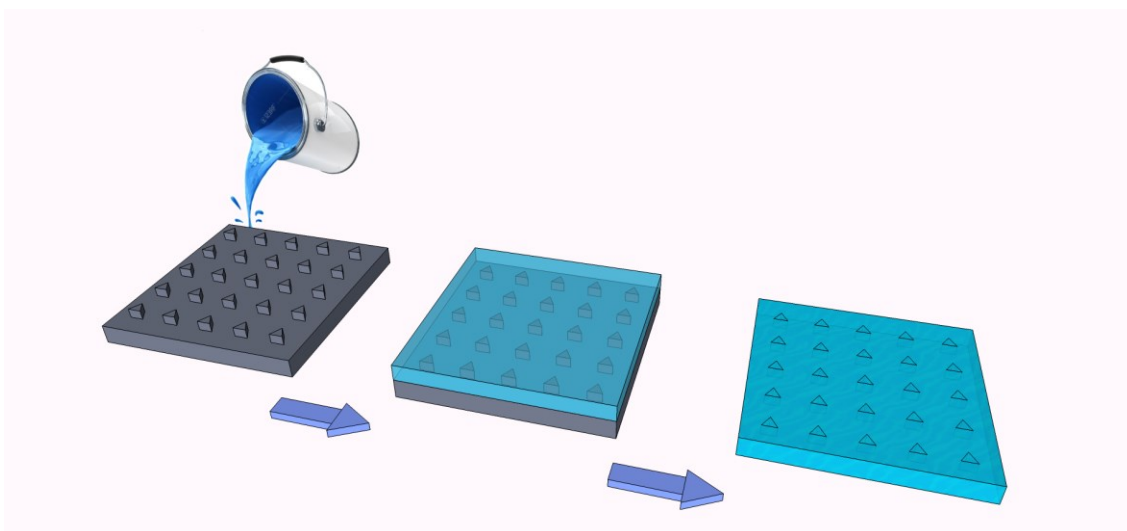
Figure 7. Typical process to produce an elastomeric stamp. A material in liquid form (e.g. PDMS), is poured onto the master and allowed to cure. After curing, the newly shaped solid material is separated from the master. The resulting stamp has negative features with respect to the master.

Plasticizing setup: A jacketed Drechsel bottle connected to a thermostatic bath and to a nitrogen line was used to vaporize the DMC/EtOH liquid solution. The temperature of the thermostatic bath was set to 25 °C while the nitrogen pressure was 0.1 bar. The ends of a flexible tube were connected to the gas outlet of the Drechsel bottle and to a glass funnel, respectively, so that the major base of the latter could lie onto the elastomeric stamp. Proper plasticizing mixture had a DMC mass fraction ranging from 0.105 to 0.165, while exposure time ranged from 1 to 7 min. Such mixtures were vaporized onto the microspheres located inside the mold cavities. The plasticizing setup is schematically shown in Figure 8.
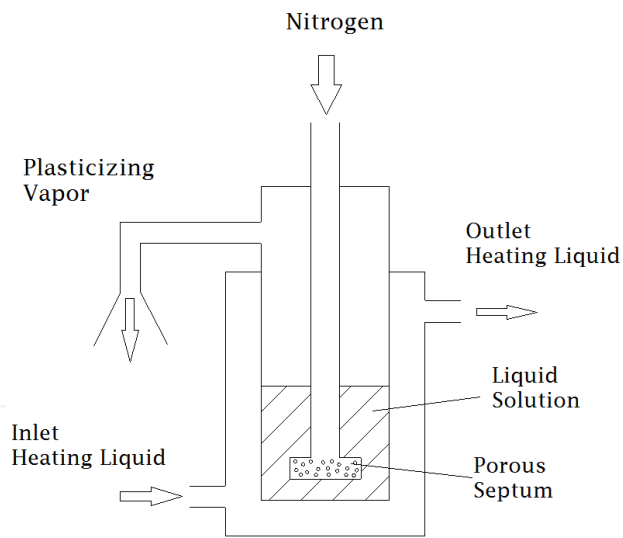
Figure 8. Plasticizing setup

Particle Plasticization

Background

The term *plasticization* is attributed to all the processes leading to a decrease in the glass transition temperature Tg of glassy polymers. It can be justified by the existence of a relationship between the yield stress σ_y and Tg.[69] The magnitude of yield stress is a measure of the resistance to plastic deformation and a Tg decrease leads to a yield stress decrease and thus makes plastic deformation easier.

Plasticization can be due to the presence of absorbed penetrants (also called diluents), e.g. water or solvents, in glassy polymers, and this phenomenon is also known as solvent plasticization. In particular, low molecular weight penetrants can increase the mobility of macromolecules.

One of the first thermodynamic models to predict the depression of Tg due to absorbed penetrants was proposed by Gibbs and Di Marzio,[70] which modeled the polymer-penetrant system using a lattice fluid theory which allows for the presence of vacant sites. This theory identifies the glass transition temperature for pure polymers and polymer-penetrant mixtures as the point, at fixed composition and pressure, at which the configurational entropy becomes zero. In other words, the Tg of a polymer-

penetrant mixture can be obtained by equating to zero the configurational entropy at a fixed pressure and composition.[63]

Other models, which rely on this equilibrium thermodynamic framework, have been described, such as those proposed by Chow[64], Gordon[71], Ellis and Karasz[72], until to the more recent works of Panayotou[73]. We were particularly interested in the Chow model, mainly because it is based on relatively easily accessible parameters as compared to other models.

Indeed, according to Chow model, the glass transition temperature is related to non-dimensional parameters which are a function of the molecular weight and concentration of diluent, number of lattice sites, monomer molecular weight, and transition isobaric heat capacity increment of the polymer. The theoretical equation proposed by Chow was also in good agreement with experimental data.

According to Chow model, prediction of the depression of Tg is described as follows:

$$ln \frac{(Tg)}{(Tg0)} = \beta[(1-\theta)ln(1-\theta) + \theta ln\theta]$$

$$\theta = \frac{Mp}{zMd}\frac{\omega}{1-\omega}$$

$$\beta = \frac{zR}{Mp\Delta Cp}$$

where Tg0 and Tg are the glass transition temperature of the pure polymer and the glass transition temperature at a given mass fraction *w (mass of the solvent/mass of the solvent+polymer)* of solvent, respectively; Mp and Md are the molecular weights of the monomer and diluent, respectively; ΔCp is the change in specific heat of the polymer associated with its glass transition temperature; R is the gas constant; and z represents the number of macromolecules in contact with a single diluent molecule, i.e. the lattice coordination number, which can alternatively be 1 or 2.

Evaluation of the Chow model parameters for PLGA 504H-DMC and NR loaded microspheres-DMC

In order to apply the Chow equation, the monomer molecular weight (65 g/mol) and the solvent molecular weight (90,08 g/mol) were retrieved from literature, whereas the Tg0 and ΔCp were experimentally determined via DSC measurements (Figure 9). In order to be consistent with units, the ΔCp value obtained from DSC was converted dividing by the heating rate (10 °C/min) and multiplying by 60 (s).

Calculations to apply the Chow equation were carried out with the aid of a spreadsheet and results are summarized in Table 1, Table 2, Figure 10, and Figure 11.

Differential Scanning Calorimetry (DSC)

Glass transition temperature and the associate change in specific heat for stock PLGA as well as for NR loaded microspheres were determined by differential scanning calorimetry (DSC) (Q20 DSC, TA Instruments).

Measurements were carried out under a constant nitrogen flow of 50 cm^3/min. Approximately 7 mg of each sample were placed in a sealed aluminum pan and dynamic DSC tests were carried out over the temperature range 10–80 °C, at an heating rate of 10 °C/min, with two heating cycles.

Figure 9, a,b, show a DSC thermogram of stock PLGA and NR loaded microspheres, respectively.
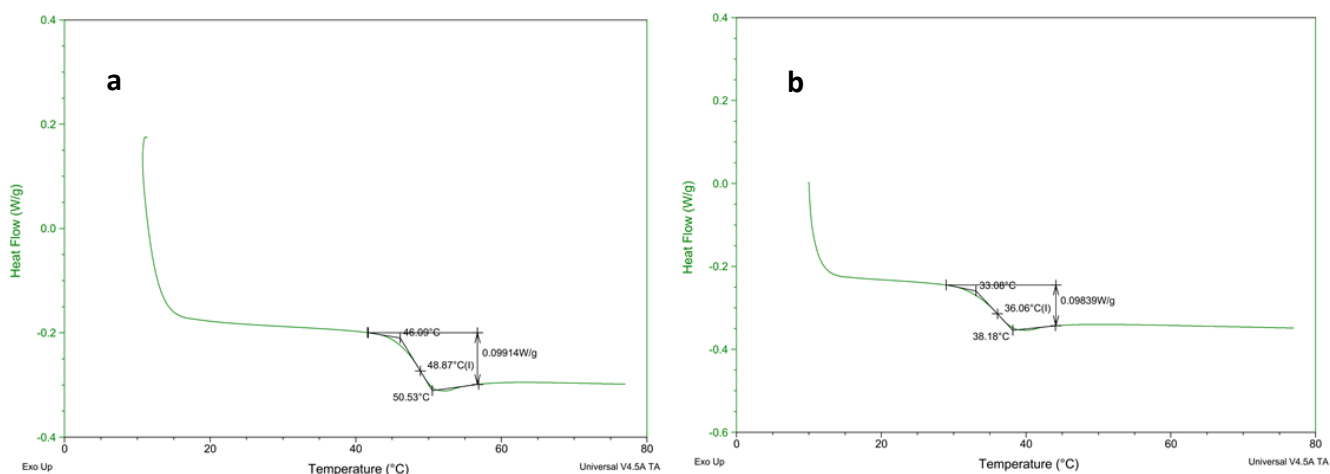
Figure 9. Differential Scanning Calorimetry (DSC) thermogram of stock PLGA RG504H (a) and NR loaded microspheres.

Chow model for stock PLGA RG504H-DMC and NR loaded microspheres-DMC

Table 1

Stock PLGA *Tg0= 322,02 K* *ΔCp= 0,59484 J/(g K)* *Mp= 65 g/mol* *Ms= 90,08 g/mol* *R= 8,3145 J /(mol K)*		z=1		z=2	
		β= 0,2150		β= 0,4301	
w	**w/(1-w)**	**θ**	**Tg**	**θ**	**Tg**
0	0,0000	0,0000	322,02	0,0000	322,02
0,02	0,0204	0,0147	316,75	0,0074	316,05
0,04	0,0417	0,0301	312,81	0,0150	311,39
0,06	0,0638	0,0461	309,34	0,0230	307,19
0,08	0,0870	0,0627	306,19	0,0314	303,27
0,1	0,1111	0,0802	303,26	0,0401	299,54
0,12	0,1364	0,0984	300,51	0,0492	295,97
0,14	0,1628	0,1175	297,91	0,0587	292,51
0,16	0,1905	0,1374	295,46	0,0687	289,15
0,18	0,2195	0,1584	293,14	0,0792	285,88
0,2	0,2500	0,1804	290,94	0,0902	282,68

Table 2

NR loaded microspheres *Tg0= 309,21 K* *ΔCp= 0,59034 J/(g K)* *Mp= 65 g/mol* *Ms= 90,08 g/mol* *R= 8,3145 J /(mol K)*		z=1		z=2	
		β=0,2167		β=0,4334	
w	w/(1-w)	θ	Tg	θ	Tg
0	0,0000	0,0000	309,21	0,0000	309,21
0,02	0,0204	0,0147	304,11	0,0074	303,44
0,04	0,0417	0,0301	300,30	0,0150	298,93
0,06	0,0638	0,0461	296,95	0,0230	294,87
0,08	0,0870	0,0627	293,89	0,0314	291,07
0,1	0,1111	0,0802	291,06	0,0401	287,47
0,12	0,1364	0,0984	288,40	0,0492	284,01
0,14	0,1628	0,1175	285,89	0,0587	280,67
0,16	0,1905	0,1374	283,52	0,0687	277,42
0,18	0,2195	0,1584	281,27	0,0792	274,26
0,2	0,2500	0,1804	279,15	0,0902	271,16
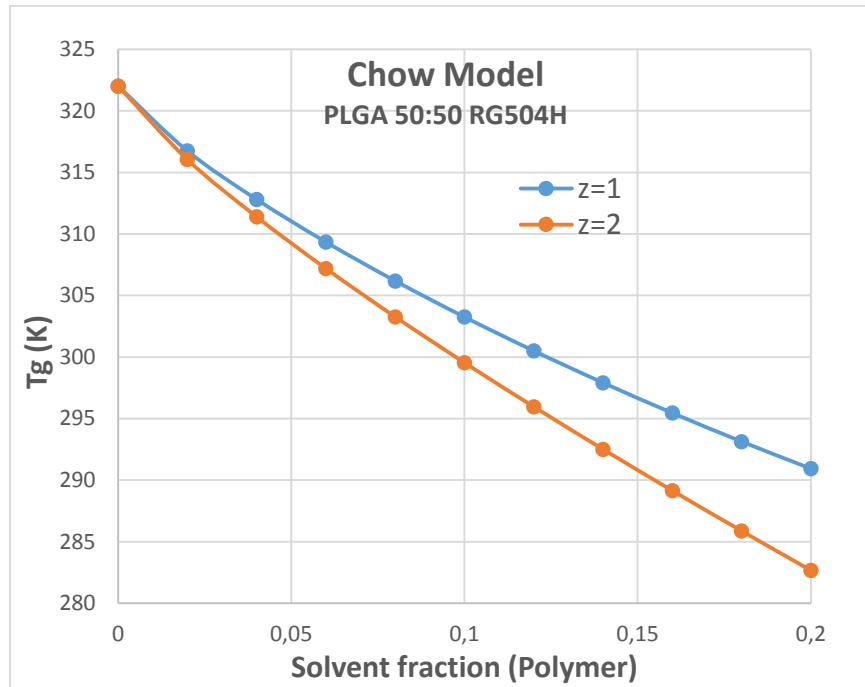
Figure 10. Chow model for stock PLGA
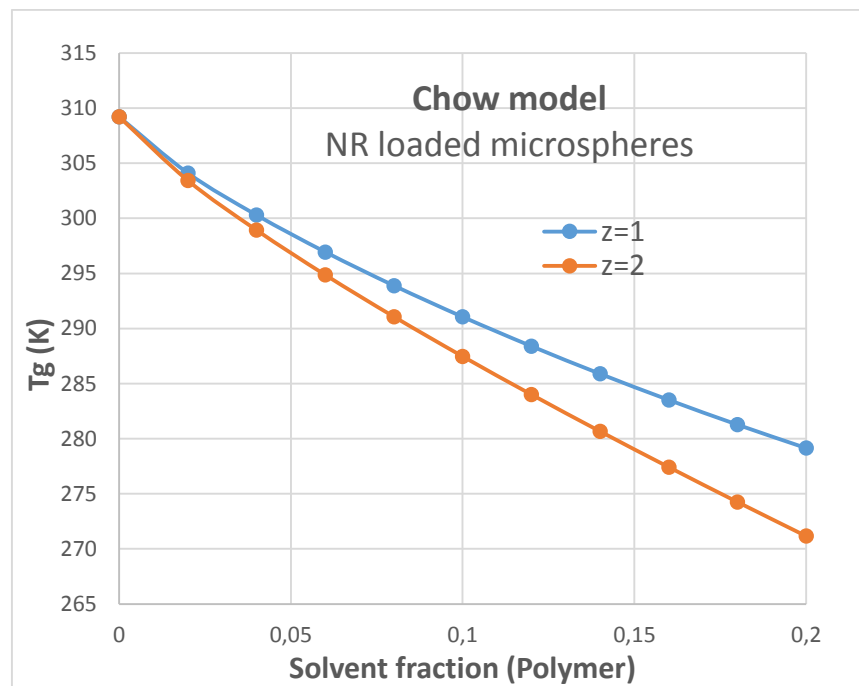
Figure 11. Chow model for NR loaded microspheres

Comparing Figure 10 and 11, it can be seen that for a given solvent fraction within the polymer, the Tg of the NR loaded microspheres is lower than that of stock PLGA.

Measurements with Quartz Crystal Microbalance (QCM)

Background

A quartz crystal microbalance is a mass sensing device with the ability to measure very small mass changes on a quartz crystal resonator in real-time. The sensitivity of the QCM is approximately 100 times higher than an electronic fine balance with a sensitivity of 0.1 mg.

QCM is based on the inverse piezoelectric effect discovered by the Curies in the late 19th century: application of voltage results in mechanical deformation of the material for crystalline materials with certain symmetry properties, such as quartz crystals cut at different orientations from the bar of quartz in order to realize specific desirable characteristics. The heart of the QCM is a piezoelectric AT-cut quartz crystal – which has nearly zero frequency drift with temperature around room temperature - sandwiched between a pair of electrodes.

When the electrodes are connected to an oscillator and an AC voltage is applied over the electrodes the quartz crystal starts to oscillate at its resonance frequency, or multiples thereof called overtones, or harmonics, due to the piezoelectric effect.[74]

Depending on the cut of the crystal relative to its crystallographic axes, different kinds of oscillations may arise. AT-cut crystals, used in QCM, vibrate in the so-called thickness-shear mode, where the two surfaces move in an antiparallel fashion. In liquids and gases, shear-waves decay rapidly, making QCM interface-specific. There are several ways to perform QCM measurements.[65] One can examine the polarization at the crystal surface as a function of the frequency of the applied voltage, the so-called impedance analysis, or QCM-Z.

An alternative is the "ring-down" scheme developed by Rodahl et al.,[75] referred to as QCM-D, where the external driving voltage is turned off intermittently and the oscillations are left to decay freely. Given that quartz is piezoelectric, a voltage is generated during these decaying mechanical oscillations. In the present study, a QCM with impedance analysis, in particular a KSV QCM-Z500, was employed.

The measurements performed with impedance analysis of the quartz crystal involves that the quartz crystal is not resonating all the time, but the crystal is swept with potential perturbations with various frequencies close to the quartz crystal's resonant frequency.[76] The potential (U) over the crystal and the electricity (I) flowing through the crystal are recorded. The ratio of U and I then give the impedance

(Z), and the result of the sweep is the so-called impedance curve (the inverse curve is called admittance).

The impedance (or admittance) curve holds all of the information concerning the properties of the quartz crystal and the layer deposited on the crystal. This sweep can be done as a function of time, which enables the measurement of mass changes happening at the quartz crystal electrode surface. The KSV QCMZ500 enables fast real-time monitoring of adsorption processes and kinetics.

Furthermore, such microbalance can measure the dissipation (D) and different harmonics of the quartz crystal giving additional information on the state of the coating, i.e. a sample, on the quartz crystal surface.

The linear relationship between changes in the resonator mass and in the resonance frequency was derived by Sauerbrey[65,77].

In particular, if the layer deposited on the crystal surface is rigid and homogeneous, the resonant frequency will decrease proportionally to the mass of the adsorbed layer according to the Sauerbrey equation:

$$\Delta f_n = -n\frac{\Delta m}{C}$$

where C is the mass-sensitivity constant, and n = 1, 3, 5… is the overtone number.

According to Sauerbrey, still under the rigid film situation, the overtone frequencies change do overlap one another.

Conversely, when the film is soft and not fully coupled with the crystal oscillations, Δf_n values measured for different overtones do not overlap. This experimental behavior is due to energy losses (or dissipation) in the system which is monitored.[76]

Much of the pioneering work in liquid phase QCM measurements has been done by Kanazawa and Gordon,[78] who showed that the change in resonant frequency and the change in dissipation of a QCM taken from air into a liquid are both proportional to the square root of the liquid's density-viscosity product:

$$\Delta f_n = -\frac{f_n}{2}\Delta D_n = -\frac{1}{C}\sqrt{\frac{n\rho_L\eta_L}{2\,\omega_F}}$$

where

ω_F is the angular fundamental resonance frequency, ρ_L is the density of the liquid and η_L is viscosity of the liquid, and ΔD_n is the dissipation change registered at the nth overtone .

In particular, it states that the decrease in the frequency and the increase in the dissipation are both proportional to the square root of the product of liquid viscosity and density. Therefore, QCM is sensitive to the properties of the bulk liquid, and when performing measurements on a film in liquid, a reference measurement in the same liquid is always necessary for separating bulk liquid contribution from the film properties.

If $\Delta D > 0$, then the film is sufficiently soft and sufficiently thick for the QCM to become sensitive to the mechanical or, more precisely, viscoelastic properties of the film.

These properties are commonly represented by the complex shear modulus $G = G' + iG''$, where i is the imaginary unit (the square root of -1).[65,79]

The storage modulus G' describes material elasticity, i.e., the relationship between applied force, or stress, and the extent of deformation, or strain. It can be thought of as a spring constant. Quantity G' is in phase with the strain and is called storage modulus, because it defines the energy stored in the sample due to the applied strain.

The loss modulus $G'' = \omega\eta$ describes viscous energy dissipation in the material subjected to deformation, where the viscosity η can be thought of as a friction coefficient that relates the applied force to the rate of deformation. The quantity G'' is out of phase with the strain and defines the dissipation of energy and is called the loss modulus. The ratio of these two quantities is called loss factor, that is $\tan\delta = G''/G'$. Typically, around Tg it is observed a well-defined peak in $\tan\delta$, accompanied by a strong decrease in E′, and it is associated to the occurrence of the glass transition.

By way of example, literature results[80] of measurements performed with a dynamic mechanical analysis, which is different from QCM, are reported in Figure L8, which depicts the above mentioned trend of G' and tanδ. Samples in that study were made of PLLA with different features, with purposes which go beyond the scope of this work.
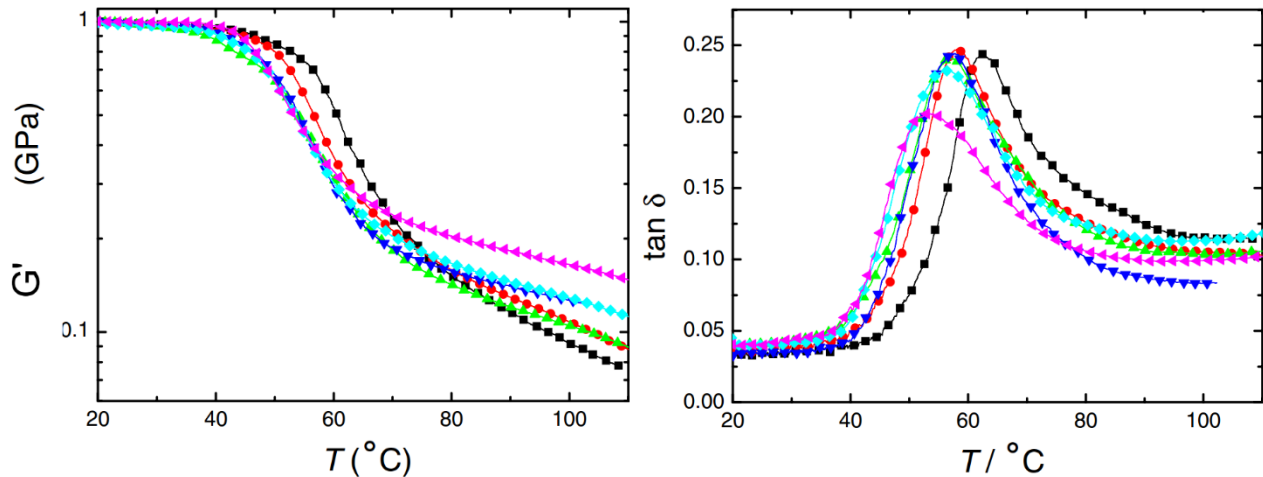

Figure L8. Trend of G' (left) and tanδ=G''/G' (right) when crossing the glass transition temperature Tg

For thin films (film thickness much thinner than the wavelength of the shear-acoustic wave in the film), frequency and dissipation shifts are related to the viscoelastic properties of the film.[65]

Summarizing, the QCM has been employed in this work because:

- It can provide a measure of the mass absorbed by a film, such as the solvent absorbed by a PLGA film, since a relationship between frequency and mass changes exists;

- It can provide information on the viscoelastic properties of the film, which are related to the glass transition, by observing the dissipation changes and eventual overtone superimposition.

Methods

Sorption of DMC by PLGA at room temperature was monitored via quartz crystal microbalance (QCM), by successively exposing a thin polymer film to DMC/EtOH solutions with equally increasing DMC mass fraction for each injection

Measurements were performed with a computer controlled quartz crystal microbalance with impedance analysis (KSV QCM-Z500) using gold-coated sensors (Q sense, 5MHz AT-cut quartz crystal).

As mentioned, such microbalance can measure the dissipation (D) and different harmonics of the quartz crystal giving additional information on the state of the PLGA film on the quartz crystal surface.

Sample preparation

Sensors were cleaned by immersion in ammonia/hydrogen peroxide solution (2:3, v/v) at 50 °C for 5 min and then spin coated with a stock-PLGA/DMC solution (25 mg/ml) at 2400 rpm for 120 s. In order to measure the resulting PLGA film thickness, a small area of the polymer was carefully scratched with the aid of a scalpel until reaching the gold substrate. The stylus of a profilometer (Veeko Dektak 150), was allowed to move from a coated area to the scratched area, so that the height difference, i.e. the film thickness, could be detected. This procedure was repeated for three samples and measured film thickness was 236 nm ± 15. A typical result of a thickness measure is shown in Figure 12.
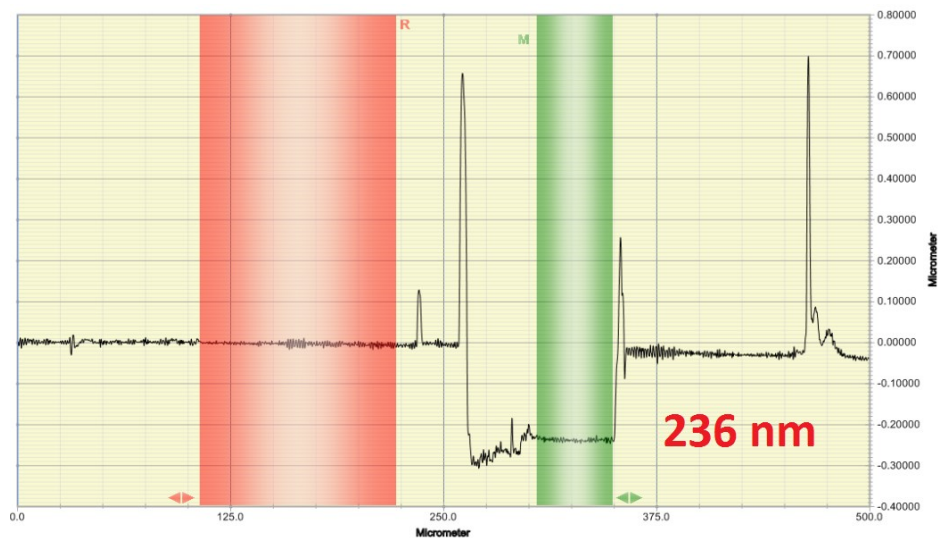
Figure 12. Thickness of a PLGA film onto a QCM sensor

Since a suitable film thickness was obtained, samples for QCM measurements were prepared with the above procedure.

Preparation of the solutions to be injected

A set of 12 DMC/EtOH solutions with DMC mass fraction in the range 0.025-0.245 with 0.02 increment were carefully prepared.

In order to prepare the DMC/EtOH solution for each injection, the required EtOH/DMC volume ratios were determined. Calculations were carried out at each desired DMC mass fraction within solution, with the aid of a spreadsheet and considering the following relationships:

$$x_{DMC}^W = m_{DMC}/m_{tot}$$

where

x_{DMC}^W is the DMC mass fraction, (i.e. $x_{DMC}^W + x_{EtOH}^W = 1$), and

m_{tot} is the total mass of the mixture, i.e. $m_{tot} = m_{DMC} + m_{EtOH}$

$$x_{DMC}^V = \frac{x_{DMC}^W \cdot \left(\frac{m_{tot}}{\rho_{DMC}}\right)}{x_{DMC}^W \cdot \left(\frac{m_{tot}}{\rho_{DMC}}\right) + x_{EtOH}^W \cdot \left(\frac{m_{tot}}{\rho_{EtOH}}\right)}$$

where:

x_{DMC}^V is the DMC volume fraction, (whereby $x_{DMC}^V + x_{EtOH}^V = 1$),

$\rho_{DMC} = 0,10635\ g\ cm^{-3}$ and $\rho_{EtOH} = = 0,785\ g\ cm^{-3}$, are the density of DMC and EtOH at 298,15 K, respectively.[81]

Results are summarized in Table 3.

Table 3

Injection	DMC Mass Fraction	EtOH Mass Fraction	DMC Volume Fraction	EtOH Volume Fraction	Volume Ratio (EtOH/DMC)
1	0,025	0,975	0,019	0,981	52,8
2	0,045	0,955	0,034	0,966	28,8
3	0,065	0,935	0,049	0,951	19,5
4	0,085	0,915	0,064	0,936	14,6
5	0,105	0,895	0,080	0,920	11,5
6	0,125	0,875	0,095	0,905	9,5
7	0,145	0,855	0,111	0,889	8,0
8	0,165	0,835	0,127	0,873	6,9
9	0,185	0,815	0,144	0,856	6,0
10	0,205	0,795	0,160	0,840	5,3
11	0,225	0,775	0,176	0,824	4,7
12	0,245	0,755	0,193	0,807	4,2

QCM measurements

Instrument temperature control was set to 25 °C and the measurement started with dry crystal. EtOH and different DMC/EtOH solutions were subsequently injected in the measurement chamber every 18 min, so that the system was suitably stabilized. The last injection, at the highest DMC mass fraction, was followed by a "washing" injection of EtOH only. Measurements were carried out monitoring different harmonics on three different samples.

The same procedure was used with an uncoated sample.

Results

The instrument software provided curves showing the mass, frequency and dissipation changes over time, i.e. at each injection.

Mass change values were collected analyzing the 7th harmonic (normalized). Similar values were obtained with different harmonics when normalized with the software instrument. In particular, mass change values at about the last minute of each injection were annotated for each sample, and the value at the last minute of the first EtOH injection was considered as a reference point for further calculations. A typical mass change VS time plot is shown in Figure 13, where the values of the dry crystal were hidden.
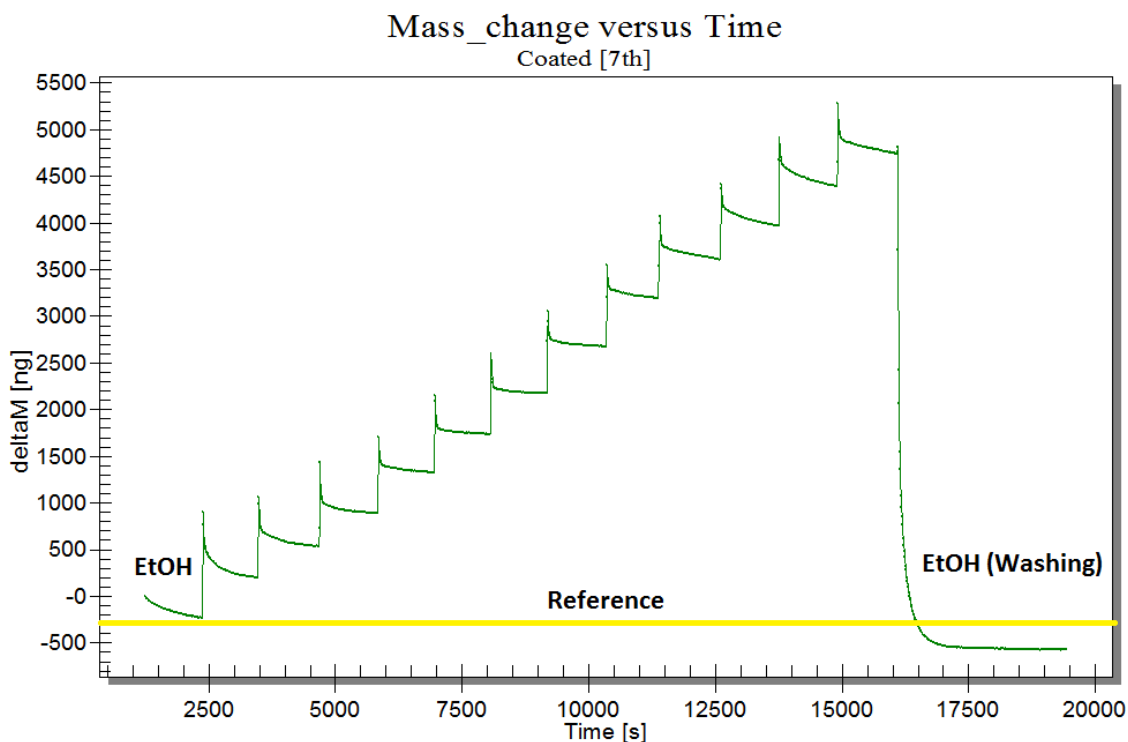
Figure 13. Mass change at each injection VS time

It can be appreciated that the registered mass increment, i.e. the amount of DMC absorbed by the PLGA film, increases substantially equally at each injection. Furthermore, it is of interest that the mass value registered at the washing injection is just slightly lower as compared to the reference value. This denotes that the PLGA film was minimally dissolved after all the injections, and presumably the dissolution occurred at the last injections due to their higher solvent concentration.

Mass change results of the measurements carried out on an uncoated crystal, not shown, did not show significant mass variation over time, thus such values were not taken into account for further calculations.

Similarly, dissipation change values were collected analyzing the 7th harmonic (normalized). In particular, dissipation change values at about the last minute of each injection were annotated for each sample.

A typical dissipation change VS time plot provided by the instrument software is shown in figure X, where the values of the dry crystal were hidden. Figure 14 shows both the dissipation change vs time plot of a coated (green) and an uncoated (blue) crystal.
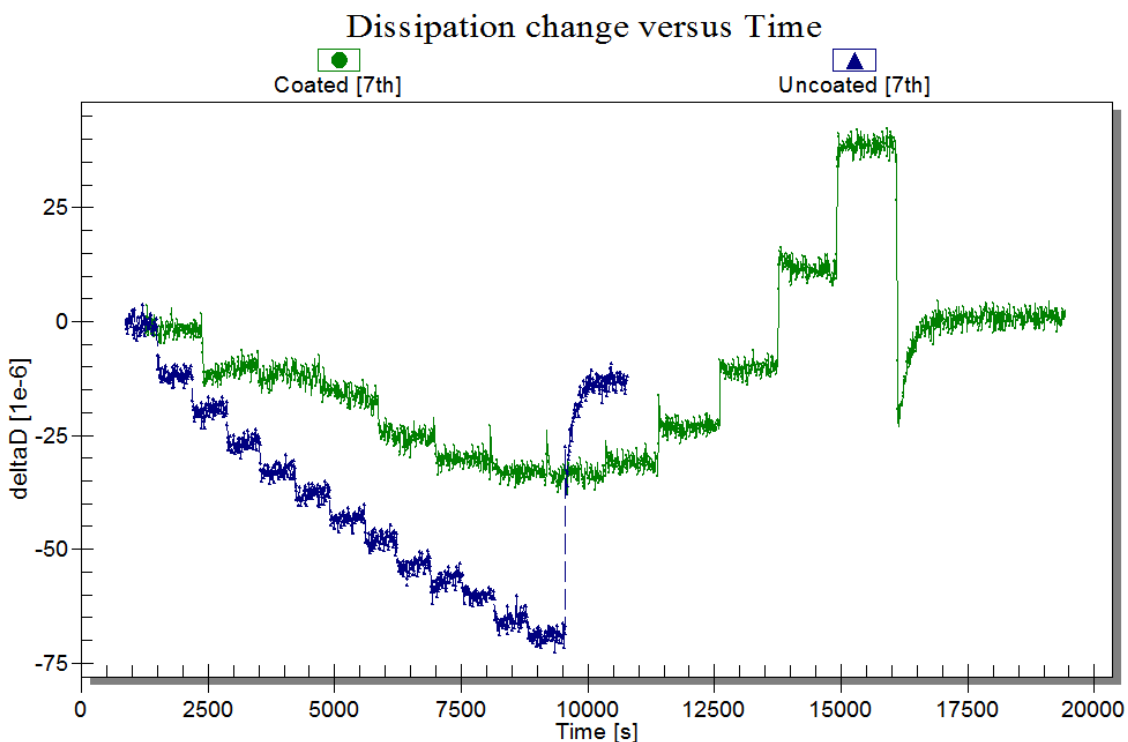
Figure 14. Dissipation change vs time plot of a coated (green) and an uncoated (blue) crystal

Referring to the coated sample, the dissipation values have a slightly decreasing trend until the seventh injection, to rise at values higher than the reference value (at the first EtOH injection) only at the eleventh injection. However, referring now to the uncoated sample, it can be seen that the dissipation values monotonically decrease with injections, and this trend is related to the solutions properties. Indeed, as mentioned, QCM measurements carried out in liquids are affected by the product of the liquid density and viscosity, and in fact a plot of data retrieved from the literature[81], Figure 15 below, shows a decreasing trend of such product with increasing DMC mole fraction.
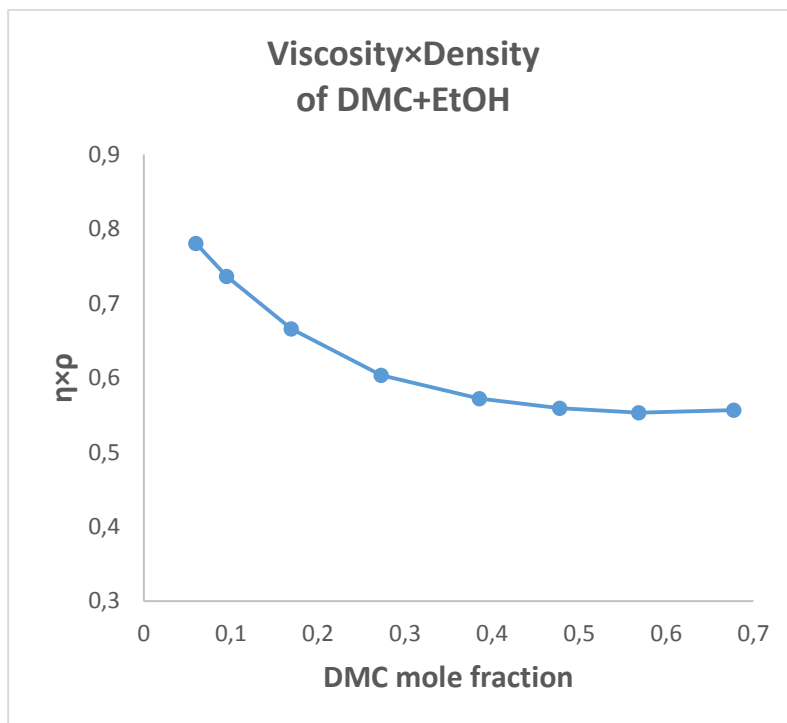
Figure 15. Plot of data retrieved from the literature

Therefore, the value registered at each injection of the uncoated sample was subtracted from the value registered for the coated sample at the corresponding injection.

Results of such calculation, reported as a mean with standard error of the three experiments performed, are reported in Figure 16.
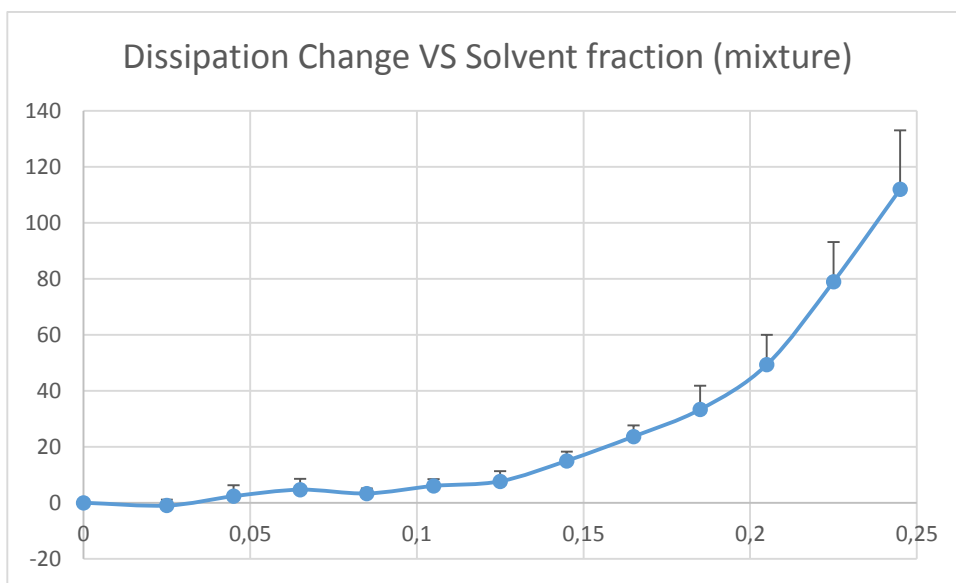
Figure 16. Dissipation change at each injection

Dissipation change ΔD appears to be substantially null until approximatively the sixth injection, where it starts to increase to values greater than zero.

In addition, the frequency change monitored for the third to the eleventh overtone also provided interestingly information. Indeed, as shown in Figure 17, while at the first injections the overtones substantially overlap, this behavior does not hold for further injections. Indeed, as the solvent mass fraction increases, the non-overlap of the harmonics is amplified, denoting that the polymer film is soft, as discussed above.
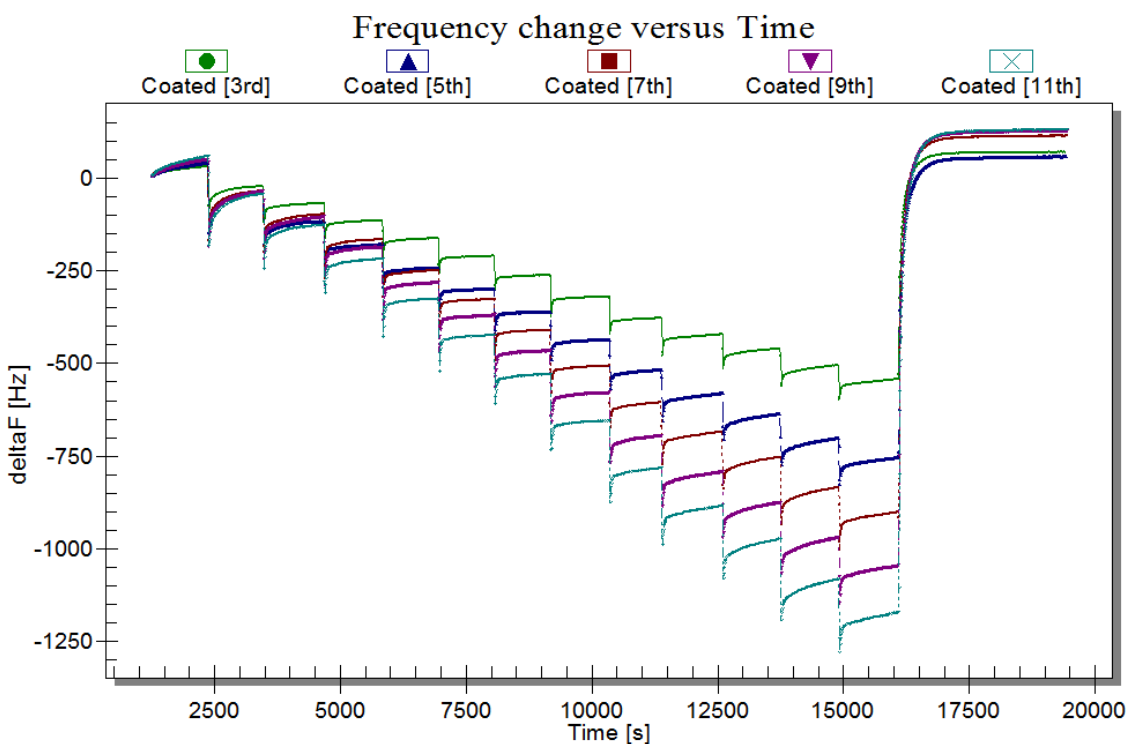
Figure 17. Frequency change monitored for different overtones over time

Data analysis

The weight of the polymer film was calculated taking into account film thickness, sensor measurement area (0.8 cm^2), and polymer density (1.23 g cm^{-3}). Solvent fraction in the polymer at each injection was calculated using the mass change registered by the instrument at the 7th harmonic (normalized) and taking into account the calculated initial polymer weight. Results relative to three different experiments are summarized in Figure 18, with related standard error.
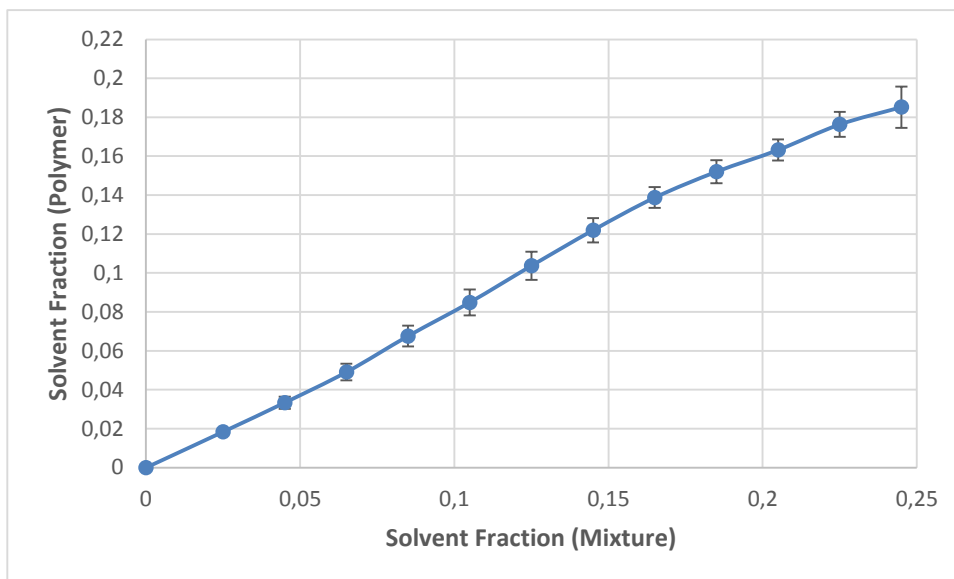
Figure 18. Solvent fraction absorbed by the polymer at each injection

Interestingly, the mean mass loss registered after the last EtOH injection was approximately 3.5% of the initial polymer mass, denoting that just a slight dissolution of the polymer film occurred.

SUPPLEMENTARY SECTION

This section includes implementations and variants of the new method.

Polymer Microneedles for transdermal drug delivery

As previously discussed, needle shaped particles are of particular interest for transdermal drug delivery. Therefore, small arrays of microneedles were produced according to the method proposed. Since microneedles are typically employed in association with patches for transdermal drug delivery, microneedles were demolded and attached to different substrates, or backings, to provide an assembly of this type. Ideally, a skin compliant, flexible substrate should be employed; furthermore, in order to minimize the time a patient should wear a patch, it would be desirable that microneedles detach from the substrate once inserted into the skin[39,82]; thus experiments were performed to this end. Finally, insertion tests into model materials, i.e. wax and gelatin, were performed.

Internally porous PLGA microspheres were produced with a Micropore® system as previously reported; microspheres were then deformed into particles with the shape of a parallelepiped with a pyramid on top. The deformation process was performed at room temperature, using a plasticizing mixture having a DMC to EtOH ratio of 1:8 (v/v) for an exposure time of 8 min. As shown in previous Figures 2, 3, and in Figure 19, microneedles were internally porous.
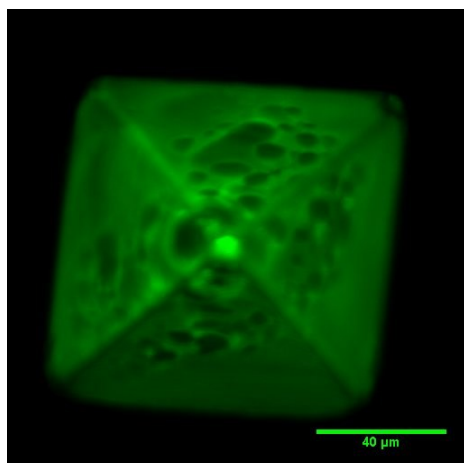
Figure 19. Confocal image of a microneedle

Various substrates were employed to demold microneedles.

First experiments were performed with a PDMS substrate patterned with protruding pillars having a diameter of about 50 µm, thus smaller than a microneedle base, and about 30 µm height. The pitch of such pillars was equal to that of the mold employed for microneedles production. A PMMA master to produce such PDMS substrate was previously generated by means of a micromilling machine.

PDMS was chosen because it is flexible and optically transparent, so that further manipulation were allowed. In addition, in order to promote adhesion to microneedles, a 10% (w/v) solution PLGA and DMC was casted on the patterned face of the PDMS substrate, and the DMC was allowed to evaporate. Immediately after microspheres deformation, when the microneedles so produced were still soft due to solvent sorption, the PDMS substrate was aligned under a stereomicroscope, as shown in figure 20, a; in particular, each pillar was aligned to the base of a respective microneedle base and pressure was applied. Solvent evaporation from the microneedles was performed with the base in contact with microneedles. After solvent evaporation, the substrate and the mold were carefully separated; in this way, microneedles were effectively demolded, being attached to the substrate. As it can be seen from figure 20, a, b, each pillar was inside a respective microneedle. It is supposed that this arrangement could provide a reinforcing at the microneedle base which could be useful for microneedles insertion into the skin. After insertion of this assembly into gelatin, microneedles did not detach from the backing.

In this and further insertion tests, a photocurable type B gelatin (degree of substitution 64%), was employed. In order to prepare the substrate for the indentation tests, 200 mg of gelatin were dissolved in 1 ml of DI water, 0.1 ml of dimethyl sulfoxide, and 1.5 mg of photoinitiator (Darocur 1173), which is 0.75% with respect to the weight of gelatin.

Gelatin was dissolved on a hot plate at 100° C for 1 hour. After pouring the gelatin in a petri dish, it was cured under a UV lamp at 365 nm for 20 minutes.
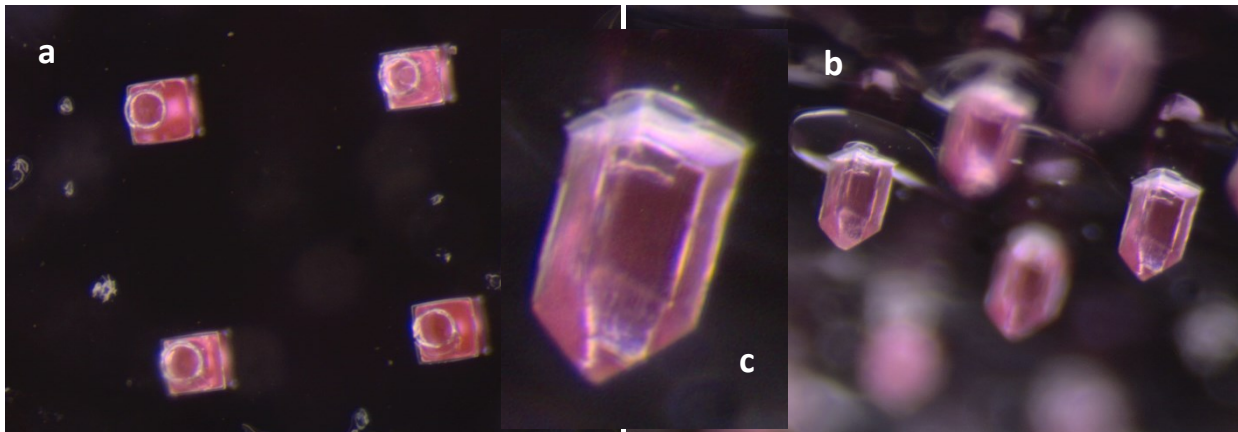
Figure 20. PDMS substrate with pillars aligned with microneedles (a). Pillars attached to the PDMS substrate with pillars inserted in each microneedle base (b, c)

A slightly different PDMS substrate was also employed. The latter had a grid of protruding channels of 30 μm height, arranged so that their intersection defined a number of squares; each square had at its center a pillar having a diameter of about 100 μm and a height of 30 μm. The negative master to produce such PDMS substrate was created by means of a micromilling machine.

A procedure similar to that described for the PDMS substrate with only pillars was employed.

The pillar diameter was selected to provide a higher surface area available for the adhesion to the microneedle base; it was supposed that the grid could serve as a spacer, thus avoiding full insertion of the pillars into the microneedles, whereby each pillar could provide a pedestal for the respective microneedle. The idea was that such arrangement could provide a higher overall length of the microneedles, and also provide an "arrow head" effect which could facilitate the microneedles detachment after insertion into the skin. Indeed, considering the geometry of the cross sections of the microneedle base and of the pillars, once attached to each other, the microneedle base slightly extended laterally beyond the respective pillar.

SEM inspection, Figure 21, of the assembly of the PDMS substrate and microneedles revealed that actually the difference between the area of microneedle base and that of the pillar was very small.
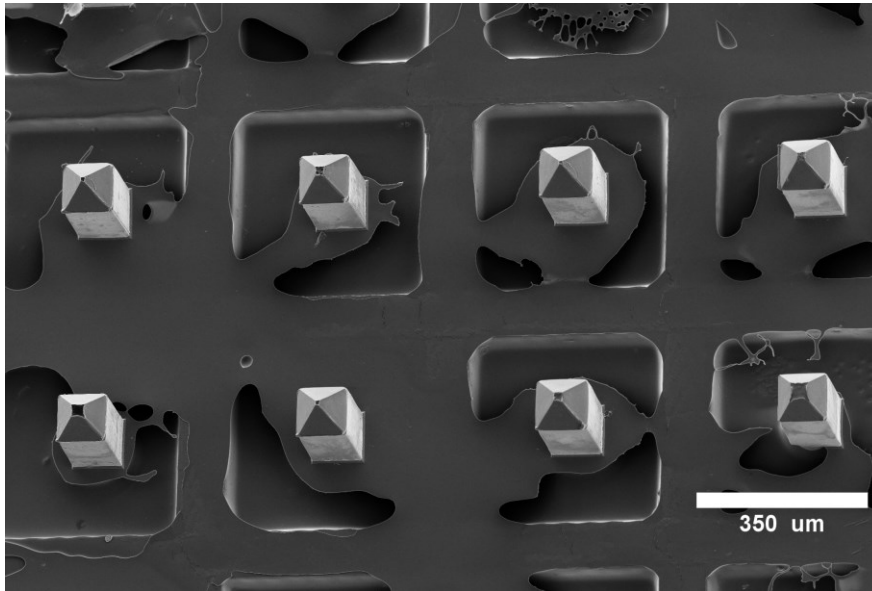
Figure 21. Assembly of the PDMS substrate with grid and pillars, and microneedles

This may account for the fact that microneedles did not detach from the PDMS substrate when inserted into gelatin. Further experiments combining the grid of channels and pillars with a smaller diameter, and/or a solution of PLGA and DMC with different concentrations could be performed.

A different approach was also used. In this case, in lieu of PLGA, two different water soluble, biocompatible adhesive were employed in order to promote the adhesion of the PDMS substrate to the microneedles. Briefly, a 10% solution of polyacrylamide (PAA) or poly-vinyl-pyrrolidone (PVP) with DI water was cast onto a flat PDMS. After microneedles production, the wet substrate was put in contact with the microneedles inside the mold cavities, and water was allowed to evaporate. After water evaporation, microneedles were effectively demolded, remaining on the PDMS substrate, as shown in figure 22, a.
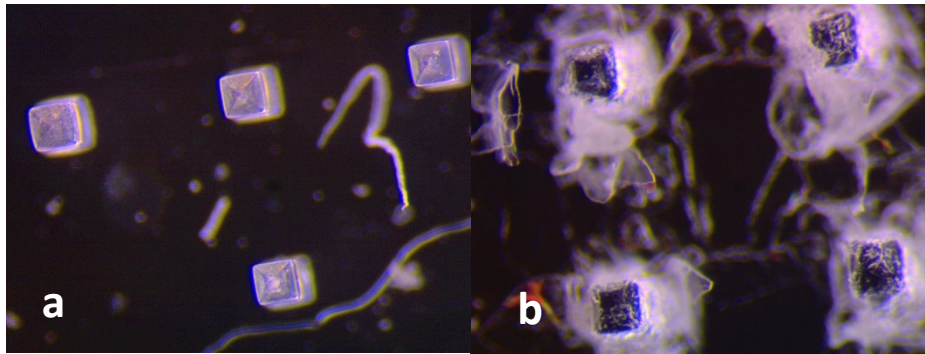
Figure 22. Microneedles onto a flat PDMS substrate coated with polyacrylamide (PAA), (a). Replica of the imprint of microneedles in paraffin wax (b)

Insertion tests were performed in gelatin and after few minutes the microneedles detached from the PDMS substrate.

Furthermore, tests were carried out in order to demonstrate the effective indentation capability of the microneedles. The indentation was performed into a small block of paraffin wax, and a PDMS replica of the microneedles imprint was observed under a stereomicrosope (Figure 22, b), to verify the effective penetration of the microneedles.

To sum up, the use of water soluble adhesive materials was the most effective to provide a detachment of the microneedles from the substrate used for demolding. Since gelatin contains a large amount of water, PAA or PVP dissolution was achieved upon hydration. A similar dissolution mechanism could occur upon insertion into the skin, due to hydration by interstitial fluid in the skin. The tests with paraffin wax, which is tougher than gelatin, demonstrated the indentation capability of microneedles. As a final remark, no significant differences between PAA and PVP at the above concentrations was observed.

Furthermore, as a proof of principle, the absorbent pad of a commercial plaster was impregnated with a solution of PAA or PVP in order to attach the microneedles to the plaster.

Sintering of PLGA microparticles

As a further study to provide a proof of principle, needle shaped microparticles were produced by sintering multiple PLGA microspheres, smaller in size, i.e. with a diameter of 5-10 µm, with respect to a single mold cavity. Such microspheres were kindly provided by Ilaria De Santo from Università degli Studi di Napoli, Federico II, CRIB department.

In order to do this, the mold cavities were carefully filled by the powder-like microspheres with the aid of a spatula. Sintering was achieved by using a 1:10 DMC/EtOH (v/v) solution, vaporized onto the particles for 10 min.

SEM inspection of the resulting particles, consisting of sintered microparticles, demolded with adhesive tape are shown in Figure 23
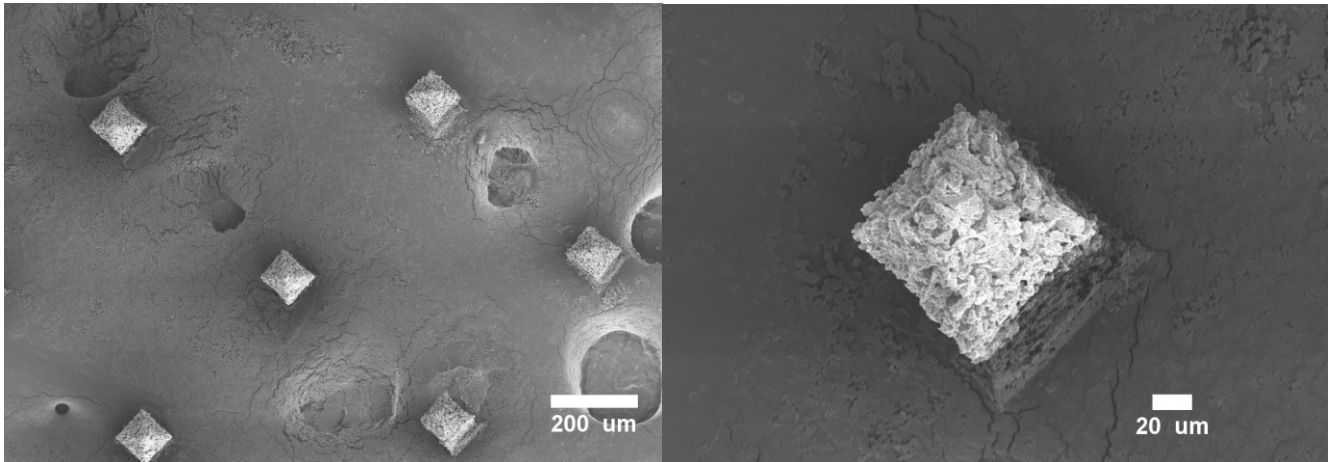
Figure 23. Sintered PLGA microspheres

Gelatin microparticles

Gelatin microspheres were provided by Francesco Urciuolo, Giorgia Imparato, and Francesca Martorina, from Istituto Italiano di Tecnologia, IIT@CRIB.

First experiments with gelatin were performed with non-porous microspheres having a diameter of about 300 μm, produced with a single emulsion technique.

Master templates made of PMMA with protruding features having the shape of cylinders, triangular and cross-shaped prism were produced with a micromilling machine. The volume of each protruding feature was substantially equal to that of a single microsphere. Briefly, a 2D CAD design (produced with Draft Sight software) with the intended geometrical shape was converted with a CAD/CAM software (Deskam 2000). The conversion was programmed in order to instruct the micromilling to machine outside the two-dimensional geometrical shape at the desired depth, so that protruding features were generated. During the process, DI water was employed as lubricant medium. The PMMA resulting substrate was carefully cleaned by brushing, in order to remove burrs.

In order to produce a mold for the microspheres, a replica was prepared by pouring PDMS monomer and curing agent (10:1) onto the master template, and allowing it to cure at 80 °C for 2 h. After peeling off the cured PDMS from the master template, the mold with reentrant features, or cavities, was ready. Microspheres were carefully positioned inside the mold cavities and the mold was then placed under the nozzle of the plasticizing setup. The latter was filled with DI water, and the thermostatic bath temperature was set to 40 °C.

Previous measurements with the plasticizing setup revealed that, when allowing the water to bubble by means of nitrogen and thus allowing the resulting water vapor to flow outside from the nozzle, the temperature at the nozzle outlet was about 25 °C. The optimal exposure time to water vapor was experimentally determined, and was about 20 min.

Inspection with a stereomicroscope, revealed that deformation was achieved. Furthermore, deformed microspheres were extracted from the mold cavities by means of an adhesive tape and SEM inspected. As it can be seen from Figure 24, even small defects of the mold cavities were transferred to the deformed microspheres, denoting a good quality of the deformation process.
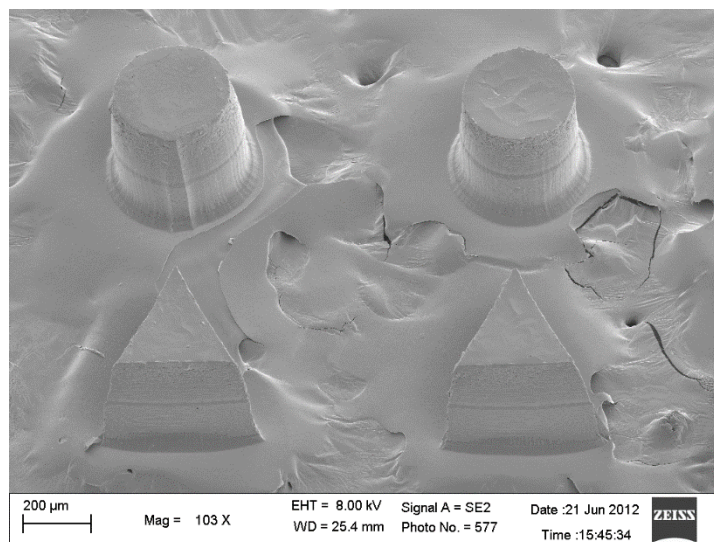
Figure 24. Shaped non-porous gelatin microparticles

Further experiments were performed with porous gelatin microspheres having a diameter of about 80 μm, produced with a double emulsion technique as previously reported. In addition, microspheres were also stabilized by means of chemical treatment with glyceraldehyde (4% w/w of microspheres), in order to make them stable in aqueous environment at body temperature. Briefly, microspheres were dispersed into an acetone/water solution containing different amounts of glyceraldehyde and mixed at 4 °C for 24 h. Then microspheres were filtered and washed with acetone and dried at room temperature.[31]

Since a higher throughput was desired, a particular design of master template was produced. Furthermore, since an aspect ratio of 3:1 could be of interest for tissue engineering purposes, size of the master features was designed accordingly. More in detail, the master was designed so that, when cured thereon, the resulting PDMS mold had cavities comprising a top portion having width equal to or larger than the microsphere diameter. This feature facilitated the filling of a lower portion of the cavities having the shape intended for the deformed microparticles, i.e. cylindrical shape with a base of 50 μm and height of about 135 μm. Figure 25 shows a SEM image of the master template.
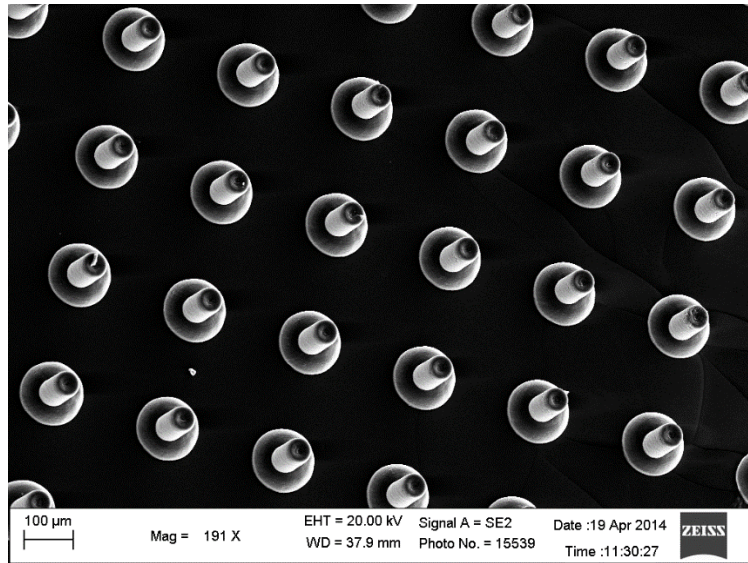
Figure 25. Master template used to produce stamps for
porous gelatin microspheres deformation

Microspheres were carefully positioned inside the mold cavities with the aid of a spatula, covering an area of the mold of approximately 1,5 x 1,5 cm^2. As above, the mold was then placed under the nozzle of the plasticizing setup, using DI water as plasticizing mixture, and the thermostatic bath temperature was set to 40 °C. The optimal exposure time was experimentally determined, and was about 10 min. Figure 26 shows SEM images of the deformed gelatin microspheres.
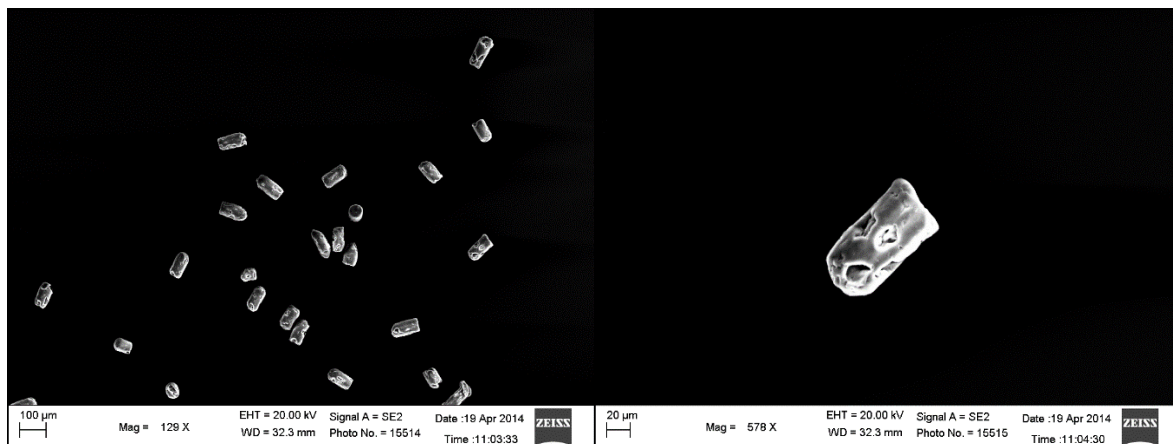
Figure 26. SEM images of porous shaped microparticles

Interestingly, the deformed microspheres had a porosity very similar to that of the starting microspheres.

Despite the good result, such microparticles could not be used for tissue engineering purposes due to

an issue related to their swelling in an aqueous environment, in particular phosphate-buffered saline (PBS). Indeed, since such microparticles were intended to be used for cells seeding, swelling tests in PBS were performed and revealed that when immersed in PBS, deformed microparticles returned a spherical shape during swelling.

In order to overcome this issue, a photocurable gelatin was used as starting material for microspheres production. Microspheres were produced with the previous double emulsion technique.

After exposure to water vapor, a previously prepared 1:1, v/v solution of EtOH and photoinitiator (Darocur 1173 or Igracure) was poured onto the deformed microparticles still inside the mold cavities and left for about 2,5 h. In particular, such solution was poured immediately after deformation, whereby the water entrapped within microparticles could facilitate the penetration of the photoinitiator. Successively, deformed microparticles were placed under a UV lamp (254 nm) for about 20 min. Then, particles were extracted from the mold cavities and swelling tests in PBS were performed. Remarkably, despite swelling and thus size increment was observed, the deformed microparticles retained their shape. Furthermore, when removing the PBS drop surrounding the microparticles, their size rapidly reduced. In particular, microparticles returned to a shape similar to their original (deformed) shape. Figure 27 shows a stereomicroscope image of deformed and photo-cured gelatin microparticles.
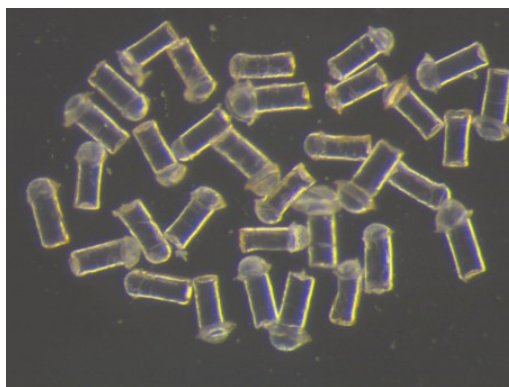
Figure 27. Deformed and photo-cured
gelatin microparticles

Figure 28 shows a comparison of the swelling behavior of the non-photocurable (first row) and photocured microparticles (second row).
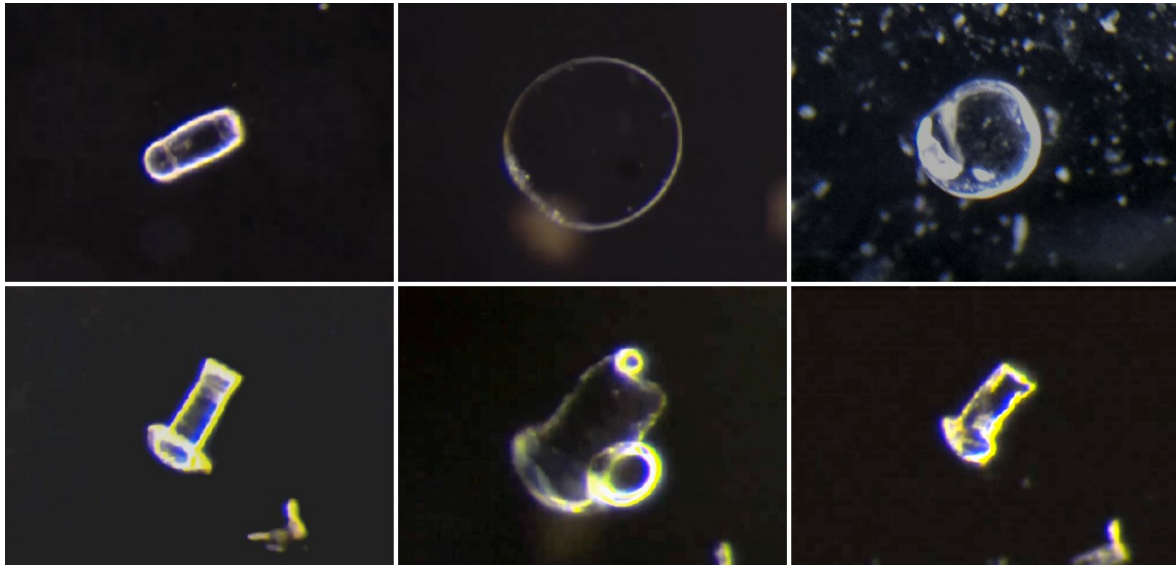
Figure 28. Comparison of the swelling behavior of the non-photocurable (first row) and photocured microparticles (second row)

However, despite the improvement, such microparticles could not be employed for tissue engineering experiments involving the seeding of cells. Indeed, when a number of deformed and photocured microparticles was left overnight in PBS – a step required for seeding cells – a particle disaggregation was observed. Typically, spherical microparticles made of non-photocurable gelatin do not show this behavior, and therefore this drawback could be attributed to the kind of gelatin the particles are made of. However, further experiments to confirm this behavior are required.

Future steps to attempt to overcome this limitation may involve a higher degree of cross-linking of microparticles. This could be achieved in several ways. For example, a solution with higher photoinitiator concentration could be employed and/or after photocuring, an additional crosslinking stage with glyceraldehyde could be provided. Alternatively, or in combination with the previous steps, a photoinitiator could be employed during starting microspheres production.

As a further study to provide a proof of principle, needle shaped microparticles were produced by sintering two (Figure 29, a) and multiple (Figure 29, b) gelatin microspheres, smaller in size with respect to a single mold cavity.
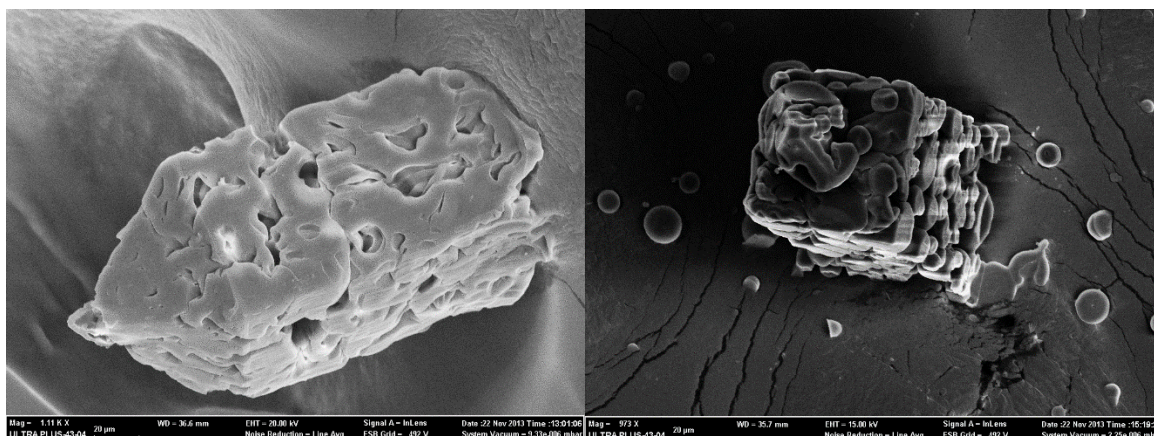
Figure 29. Sintering of two (a) and multiple (b) gelatin microparticles

Automation of the process

In order to provide an automated production process, a collecting device was fabricated to overcome the bottle neck represented by the insertion of the microspheres into the molding cavities. The proposed collecting device, and a schematic representation of its operation is shown in Figure 30.
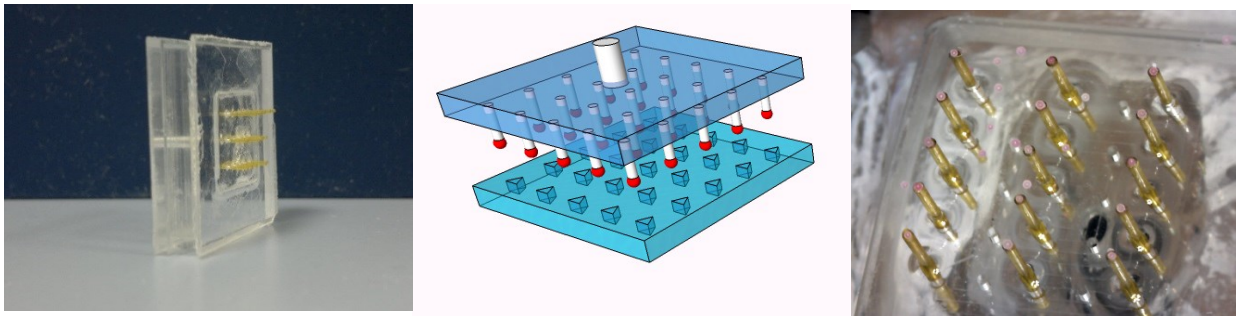
Figure 30. Collecting device and schematic representation of its operation

Briefly, two PMMA substrates (5 and 1 mm thick, respectively) were produced with a micromilling machine. The first PMMA layer was pocketed producing a first groove; the groove was drilled at its center so that a circular hole resulted.

The second PMMA layer was pocketed producing a second groove, intended to be aligned with the first groove; then the second groove was machined to produce therein an array of holes - each with a diameter of about 130 μm - with a pitch, or center-to-center distance, equal to that of the cavities of the stamp. Silica capillaries with a lumen of about 50 μm, intended to be smaller than a microsphere diameter, were then inserted in each hole and sealed with a cyanacrylate glue. A manifold, formed by a thin tube or needle, was fitted and sealed in the hole of the first PMMA substrate in the same way. The two layers were then bonded with ethanol in oven at 70° C for 1.5 h. The two facing and matching pocketed portions of the respective PMMA substrate provided a vacuum chamber.

The manifold was connected to a vacuum pump. When the vacuum pump was started, the collecting device was used to pick up a number of microspheres -one microsphere for each capillary- and enable them to be deposited in the mold cavities. In particular, after the alignment of the capillaries to the

mold cavities by means of a magnifying camera, the vacuum pump was stopped, and microspheres were released.

In order to avoid phenomena of aggregation of the microparticles due to electrostatic interactions that may occur, depending on the plastic material from which the particles are made, and in order to ensure that a single microsphere is retained at each capillary end, a small flow of air can be used, or a brushing operation can be carried out before the vacuum pump is stopped.

The same micromanipulator can be used to supply vapors of the plasticizing mixture, using a carrier gas such as nitrogen, in a localized manner on the microspheres or in the vicinity of the microspheres positioned in each mold cavity.

CONCLUSIONS

To sum up, the new method has been proven effective to produce non-spherical polymeric particles starting from previously fabricated PLGA microspheres loaded with VEGF/Hp/BSA.

Indeed, this method allows to preserve both the microstructure and molecule distribution of the starting microspheres, providing shaped microparticles that can release active VEGF over time. In particular, the shaped microparticles keep a porous microstructure and VEGF/Hp/BSA distribution similar to that of the starting microspheres, whereby the release of the VEGF embedded in the shaped microparticles and in starting microspheres is equivalent. The gentleness of the process conditions is mainly due to the use of a solvent/non-solvent plasticizing mixture at the vapor state. A valuable aspect is that this deformation technique allows to effectively exploit particle formulation strategies and drug encapsulation methods already developed and available for microspheres.

Remarkably, the retention of the biological activity of a very labile protein, such as VEGF, let to hypothesize that a wide variety of different drugs and proteins can be processed with this method.

Beside PLGA, one of the most frequently used biomaterials for microsphere production, other materials employed for drug delivery and tissue engineering are likely to be plasticized at room temperature exploiting Tg depression due to solvent sorption. This was proven by tests performed on gelatin microspheres, which were deformed at room temperature employing water as a plasticizing solvent.

The strength of this study relies on the careful evaluation not only of the VEGF quantity entrapped within microparticles, but also on the effects of the processing conditions on the VEGF bioactivity, which supports the possible use of our process to produce shaped polymer microparticles preserving the effectiveness of the embedded labile biomolecules.

Furthermore, this technique could also be employed to produce microneedles for transdermal drug delivery, since microspheres have been deformed into a specific shape for this purpose. To this end, the methods employed to demold the microparticles could be useful to provide an effective drug delivery system; indeed, microneedles were attached to a flexible substrate from which they were released when inserted into gelatin. This could similarly happen upon insertion into the skin. In addition, sintering of small microspheres (1-10 μm) to obtain larger particles by means of solvent/non-solvent plasticization was also demonstrated.

The findings of this thesis prompt further investigations to evaluate the effects of more elongated shapes on the release profiles of the embedded biomolecules, as well as the effects of the use of the shaped gelatin microparticles for tissue engineering.

Finally, this new and easy technique, which has been conceived to be effortlessly carried out starting from previously fabricated microspheres, could be appealing for scientists of different backgrounds involved in multidisciplinary research fields.

ACKNOWLEDGMENTS

APPENDIX

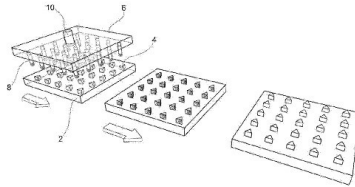(54) Title: METHOD FOR PRODUCING SHAPED POLYMERIC MICROPARTICLES

FIG.1

(57) Abstract: Method for producing shaped polymeric microparticles of non-spherical shape, comprising the steps of: placing one or more microparticles of substantially spherical shape in a respective micro-cavity of a mould having the desired non-spherical shape; subjecting said microparticles to softening by exposure to a solvent or mixture of solvent/non- solvent, in the liquid or vapour state, adapted to plasticize the polymeric mate- rial constituting said microparticles, and possibly assisting the solvent plasticization proc- ess by heat treatment, not excluding the possibility, in less critical cases in terms of con- servation of the microstructure, of car- rying out heat treatment exclusively, at a temperature not exceeding 40% of the glass transition temperature of the polymer material; and removing said microparticles from the mould cavities.

WO 2014/167495 A1

Riquadro N. VDichiarazione motivata a riguardo di novità, attività inventiva o applicazione industriale; citazioni e spiegazioni giustificative della dichiarazione

1. 1.   Dichiarazione

Novità (N)	Sì:	Rivendicazioni	1-8
	No:	Rivendicazioni	
Attività inventiva (IS)	Sì:	Rivendicazioni	1-8
	No:	Rivendicazioni	
Applicazione industriale (IA)	Sì:	Rivendicazioni	1-8
	No:	Rivendicazioni	

Since the method claimed in claim 1 is not suggested by any of the documents of the available prior art, the subject-matter of claim 1 is considered to meet the requirements of novelty and inventive step.

REFERENCES

1. Champion, J. A., Katare, Y. K. & Mitragotri, S. Particle shape: A new design parameter for micro- and nanoscale drug delivery carriers. *J. Controlled Release* **121,** 3–9 (2007).

2. Siepmann, J. & Siepmann, F. Modeling of diffusion controlled drug delivery. *J. Controlled Release* **161,** 351–362 (2012).

3. Acharya, G. *et al.* The hydrogel template method for fabrication of homogeneous nano/microparticles. *J. Controlled Release* **141,** 314–319 (2010).

4. Klose, D., Siepmann, F., Elkharraz, K., Krenzlin, S. & Siepmann, J. How porosity and size affect the drug release mechanisms from PLGA-based microparticles. *Int. J. Pharm.* **314,** 198–206 (2006).

5. Makadia, H. K. & Siegel, S. J. Poly Lactic-co-Glycolic Acid (PLGA) as Biodegradable Controlled Drug Delivery Carrier. *Polymers* **3,** 1377–1397 (2011).

6. Guan, J., Ferrell, N., James Lee, L. & Hansford, D. J. Fabrication of polymeric microparticles for drug delivery by soft lithography. *Biomaterials* **27,** 4034–4041 (2006).

7. Mitragotri, S. & Lahann, J. Physical approaches to biomaterial design. *Nat. Mater.* **8,** 15–23 (2009).

8. Muro, S. *et al.* Control of endothelial targeting and intracellular delivery of therapeutic enzymes by modulating the size and shape of ICAM-1-targeted carriers. *Mol. Ther.* **16,** 1450–1458 (2008).

9. Champion, J. A. & Mitragotri, S. Role of target geometry in phagocytosis. *Proc. Natl. Acad. Sci. U. S. A.* **103,** 4930–4934 (2006).

10. Arora, A., Prausnitz, M. R. & Mitragotri, S. Micro-scale devices for transdermal drug delivery. *Int. J. Pharm.* **364,** 227–236 (2008).

11. Prausnitz, M. R. & Langer, R. Transdermal drug delivery. *Nat. Biotechnol.* **26,** 1261–1268 (2008).

12. Lee, J. W., Park, J.-H. & Prausnitz, M. R. Dissolving microneedles for transdermal drug delivery. *Biomaterials* **29,** 2113–2124 (2008).

13. Wermeling, D. P. *et al.* Microneedles permit transdermal delivery of a skin-impermeant medication to humans. *Proc. Natl. Acad. Sci.* **105,** 2058–2063 (2008).

14. Sullivan, S. P. *et al.* Dissolving polymer microneedle patches for influenza vaccination. *Nat. Med.* **16,** 915–920 (2010).

15. Koutsonanos, D. G. *et al.* Delivery of subunit influenza vaccine to skin with microneedles improves immunogenicity and long-lived protection. *Sci. Rep.* **2,** (2012).

16. Andrews, S. N., Jeong, E. & Prausnitz, M. R. Transdermal Delivery of Molecules is Limited by Full Epidermis, Not Just Stratum Corneum. *Pharm. Res.* **30,** 1099–1109 (2013).

17. Park, J.-H., Allen, M. G. & Prausnitz, M. R. Biodegradable polymer microneedles: Fabrication, mechanics and transdermal drug delivery. *J. Controlled Release* **104,** 51–66 (2005).

18. Sullivan, S. P., Murthy, N. & Prausnitz, M. R. Minimally Invasive Protein Delivery with Rapidly Dissolving Polymer Microneedles. *Adv. Mater.* **20,** 933–938 (2008).

19. Park, J.-H. *et al.* Polymer particle-based micromolding to fabricate novel microstructures. *Biomed. Microdevices* **9,** 223–234 (2007).

20. Moga, K. A. *et al.* Rapidly-Dissolvable Microneedle Patches Via a Highly Scalable and Reproducible Soft Lithography Approach. *Adv. Mater.* **25,** 5060–5066 (2013).

21. Vecchione, R. *et al.* Electro-Drawn Drug-Loaded Biodegradable Polymer Microneedles as a Viable Route to Hypodermic Injection. *Adv. Funct. Mater.* **24,** 3515–3523 (2014).

22. Nichol, J. W. & Khademhosseini, A. Modular tissue engineering: engineering biological tissues from the bottom up. *Soft Matter* **5,** 1312 (2009).

23. Urciuolo, F., Imparato, G., Totaro, A. & Netti, P. A. BuildinG a tissue in vitro FroM the BottoM uP: iMPliCations in reGenerative MediCine. *Methodist DeBakey Cardiovasc. J.* **9,** 213 (2013).

24. Tibbitt, M. W. & Anseth, K. S. Hydrogels as extracellular matrix mimics for 3D cell culture. *Biotechnol. Bioeng.* **103,** 655–663 (2009).

25. Drury, J. L. & Mooney, D. J. Hydrogels for tissue engineering: scaffold design variables and applications. *Biomaterials* **24,** 4337–4351 (2003).

26. Lee, K. Y. & Mooney, D. J. Hydrogels for tissue engineering. *Chem. Rev.* **101,** 1869–1880 (2001).

27. Owen, S. C. & Shoichet, M. S. Design of three-dimensional biomimetic scaffolds. *J. Biomed. Mater. Res. A* **94,** 1321–1331 (2010).

28. Zorlutuna, P. *et al.* Microfabricated Biomaterials for Engineering 3D Tissues. *Adv. Mater.* **24,** 1782–1804 (2012).

29. Du, Y., Lo, E., Vidula, M. K., Khabiry, M. & Khademhosseini, A. Method of bottom-up directed assembly of cell-laden microgels. *Cell. Mol. Bioeng.* **1,** 157–162 (2008).

30. Zamanian, B. *et al.* Interface-directed self-assembly of cell-laden microgels. *Small* **6,** 937–944 (2010).

31. Imparato, G., Urciuolo, F., Casale, C. & Netti, P. A. The role of microscaffold properties in controlling the collagen assembly in 3D dermis equivalent using modular tissue engineering. *Biomaterials* **34,** 7851–7861 (2013).

32. Dendukuri, D. & Doyle, P. S. The Synthesis and Assembly of Polymeric Microparticles Using Microfluidics. *Adv. Mater.* **21,** 4071–4086 (2009).

33. Hakimi, N., Tsai, S. S. H., Cheng, C.-H. & Hwang, D. K. One-Step Two-Dimensional Microfluidics-Based Synthesis of Three-Dimensional Particles. *Adv. Mater.* **26,** 1393–1398 (2014).

34. Eydelnant, I. A., Betty Li, B. & Wheeler, A. R. Microgels on-demand. *Nat. Commun.* **5,** (2014).

35. Rogers, J. A. & Nuzzo, R. G. Recent progress in soft lithography. *Mater. Today* **8,** 50–56 (2005).

36. Xia, Y. & Whitesides, G. M. Soft lithography. *Annu. Rev. Mater. Sci.* **28,** 153–184 (1998).

37. Lee, S.-J. J. *Microfabrication for microfluidics*. (Artech House, 2010).

38. Jung-Hwan Park, Yong-Kyu Yoon, Seong-O Choi, Prausnitz, M. R. & Allen, M. G. Tapered Conical Polymer Microneedles Fabricated Using an Integrated Lens Technique for Transdermal Drug Delivery. *IEEE Trans. Biomed. Eng.* **54,** 903–913 (2007).

39. Chu, L. Y. & Prausnitz, M. R. Separable arrowhead microneedles. *J. Controlled Release* **149,** 242–249 (2011).

40. Rolland, J. P. *et al.* Direct Fabrication and Harvesting of Monodisperse, Shape-Specific Nanobiomaterials. *J. Am. Chem. Soc.* **127,** 10096–10100 (2005).

41. Rolland, J. P., Hagberg, E. C., Denison, G. M., Carter, K. R. & De Simone, J. M. High-Resolution Soft Lithography: Enabling Materials for Nanotechnologies. *Angew. Chem.* **116,** 5920–5923 (2004).

42. Wang, Y. *et al.* Generation of a Library of Particles Having Controlled Sizes and Shapes via the Mechanical Elongation of Master Templates. *Langmuir* **27,** 524–528 (2011).

43. Williams, C. G., Malik, A. N., Kim, T. K., Manson, P. N. & Elisseeff, J. H. Variable cytocompatibility of six cell lines with photoinitiators used for polymerizing hydrogels and cell encapsulation. *Biomaterials* **26,** 1211–1218 (2005).

44. Champion, J. A., Katare, Y. K. & Mitragotri, S. Making polymeric micro-and nanoparticles of complex shapes. *Proc. Natl. Acad. Sci.* **104,** 11901–11904 (2007).

45. Chen, R. R. & Mooney, D. J. Polymeric growth factor delivery strategies for tissue engineering. *Pharm. Res.* **20,** 1103–1112 (2003).

46. Li, M., Rouaud, O. & Poncelet, D. Microencapsulation by solvent evaporation: State of the art for process engineering approaches. *Int. J. Pharm.* **363,** 26–39 (2008).

47. Yang, Y.-Y., Chung, T.-S. & Ping Ng, N. Morphology, drug distribution, and in vitro release profiles of biodegradable polymeric microspheres containing protein fabricated by double-emulsion solvent extraction/evaporation method. *Biomaterials* **22,** 231–241 (2001).

48. D' Angelo, I., Oliviero, O., Ungaro, F., Quaglia, F. & Netti, P. A. Engineering strategies to control vascular endothelial growth factor stability and levels in a collagen matrix for angiogenesis: The role of heparin sodium salt and the PLGA-based microsphere approach. *Acta Biomater.* **9,** 7389–7398 (2013).

49. Borselli, C. *et al.* Bioactivation of collagen matrices through sustained VEGF release from PLGA microspheres. *J. Biomed. Mater. Res. A* **92A,** 94–102 (2010).

50. Ungaro, F. *et al.* Bioactivated polymer scaffolds for tissue engineering. *Top. Tissue Eng.* **2,** (2005).

51. Kelly, J. Y. & DeSimone, J. M. Shape-Specific, Monodisperse Nano-Molding of Protein Particles. *J. Am. Chem. Soc.* **130,** 5438–5439 (2008).

52. Saltzman, W. M. & Olbricht, W. L. BUILDING DRUG DELIVERY INTO TISSUE ENGINEERING. *Nat. Rev. Drug Discov.* **1,** 177–186 (2002).

53. Langer, R. Tissue Engineering. *Mol. Ther.* **1,** 12–15 (2000).

54. Van de Weert, M., Jorgensen, L., Horn Moeller, E. & Frokjaer, S. Factors of importance for a successful delivery system for proteins. (2005).

55. Freiberg, S. & Zhu, X. X. Polymer microspheres for controlled drug release. *Int. J. Pharm.* **282,** 1–18 (2004).

56. Khademhosseini, A. & Langer, R. Microengineered hydrogels for tissue engineering. *Biomaterials* **28,** 5087–5092 (2007).

57. Shim, T. S., Kim, S.-H. & Yang, S.-M. Elaborate Design Strategies Toward Novel Microcarriers for Controlled Encapsulation and Release. *Part. Part. Syst. Charact.* **30,** 9–45 (2013).

58. Kolhar, P. & Mitragotri, S. Polymer Microparticles Exhibit Size and Shape Dependent Accumulation around the Nucleus after Endocytosis. *Adv. Funct. Mater.* **22,** 3759–3764 (2012).

59. Best, J. P., Yan, Y. & Caruso, F. The Role of Particle Geometry and Mechanics in the Biological Domain. *Adv. Healthc. Mater.* **1,** 35–47 (2012).

60. Qi, H. *et al.* DNA-directed self-assembly of shape-controlled hydrogels. *Nat. Commun.* **4,** (2013).

61. Tasoglu, S. *et al.* Guided and magnetic self-assembly of tunable magnetoceptive gels. *Nat. Commun.* **5,** 4702 (2014).

62. Yang, S. Y. *et al.* A bio-inspired swellable microneedle adhesive for mechanical interlocking with tissue. *Nat. Commun.* **4,** 1702 (2013).

63. Mensitieri, G. & Scherillo, G. Environmental resistance of high performance polymeric matrices and composites. *Wiley Encycl. Compos.* (2012). at <http://onlinelibrary.wiley.com/doi/10.1002/9781118097298.weoc074/full>

64. Chow, T. S. Molecular interpretation of the glass transition temperature of polymer-diluent systems. *Macromolecules* **13,** 362–364 (1980).

65. Reviakine, I., Johannsmann, D. & Richter, R. P. Hearing What You Cannot See and Visualizing What You Hear: Interpreting Quartz Crystal Microbalance Data from Solvated Interfaces. *Anal. Chem.* **83,** 8838–8848 (2011).

66. Battista, E. *et al.* Ligand engagement on material surfaces is discriminated by cell mechanosensoring. *Biomaterials* **45,** 72–80 (2015).

67. Sacanna, S. *et al.* Shaping colloids for self-assembly. *Nat. Commun.* **4,** 1688 (2013).

68. Borselli, C., Oliviero, O., Battista, S., Ambrosio, L. & Netti, P. A. Induction of directional sprouting angiogenesis by matrix gradients. *J. Biomed. Mater. Res. A* **80A,** 297–305 (2007).

69. Davies, P. & Rajapakse, Y. D. *Durability of composites in a marine environment*. (Springer, 2014).

70. Gibbs, J. H. & DiMarzio, E. A. Nature of the glass transition and the glassy state. *J. Chem. Phys.* **28,** 373–383 (1958).

71. Gordon, J., Rouse, G., Gibbs, J. & Risen Jr, W. M. The composition dependence of glass transition properties. *J. Chem. Phys.* **66,** 4971–4976 (1977).

72. Ellis, T. & Karasz, F. Interaction of epoxy resins with water: the depression of glass transition temperature. *Polymer* **25,** 664–669 (1984).

73. Panayiotou, C., Pantoula, M., Stefanis, E., Tsivintzelis, I. & Economou, I. G. Nonrandom hydrogen-bonding model of fluids and their mixtures. 1. Pure fluids. *Ind. Eng. Chem. Res.* **43,** 6592–6606 (2004).

74. QCM-Z500_Manual.pdf.

75. Rodahl, M., Höök, F., Krozer, A., Brzezinski, P. & Kasemo, B. Quartz crystal microbalance setup for frequency and Q-factor measurements in gaseous and liquid environments. *Rev. Sci. Instrum.* **66,** 3924–3930 (1995).

76. Kujawa, P., Schmauch, G., Viitala, T., Badia, A. & Winnik, F. M. Construction of Viscoelastic Biocompatible Films via the Layer-by-Layer Assembly of Hyaluronan and Phosphorylcholine-Modified Chitosan. *Biomacromolecules* **8,** 3169–3176 (2007).

77. Sauerbrey, G. Verwendung von Schwingquarzen zur Wägung dünner Schichten und zur Mikrowägung. *Z. Für Phys.* **155,** 206–222 (1959).

78. Kanazawa, K. K. & Gordon, J. G. Frequency of a quartz microbalance in contact with liquid. *Anal. Chem.* **57,** 1770–1771 (1985).

79. Sideridis, E., Prassianakis, I. N. & Kytopoulos, V. N. Storage and loss moduli behavior of plasticized epoxy polymers over a frequency and temperature range, and damaging effects assessment by means of the NDT method of ultrasounds and moisture absorption. *J. Appl. Polym. Sci.* **101,** 3869–3880 (2006).

80. Picciochi, R., Wang, Y., Alves, N. M. & Mano, J. F. Glass transition of semi-crystalline PLLA with different morphologies as studied by dynamic mechanical analysis. *Colloid Polym. Sci.* **285,** 575–580 (2007).

81. Rodríguez, A., Canosa, J. & Tojo, J. Physical Properties of Binary Mixtures (Dimethyl Carbonate + Alcohols) at Several Temperatures. *J. Chem. Eng. Data* **46,** 1476–1486 (2001).

82. DeMuth, P. C., Garcia-Beltran, W. F., Ai-Ling, M. L., Hammond, P. T. & Irvine, D. J. Composite Dissolving Microneedles for Coordinated Control of Antigen and Adjuvant Delivery Kinetics in Transcutaneous Vaccination. *Adv. Funct. Mater.* **23,** 161–172 (2013).

GALLERY
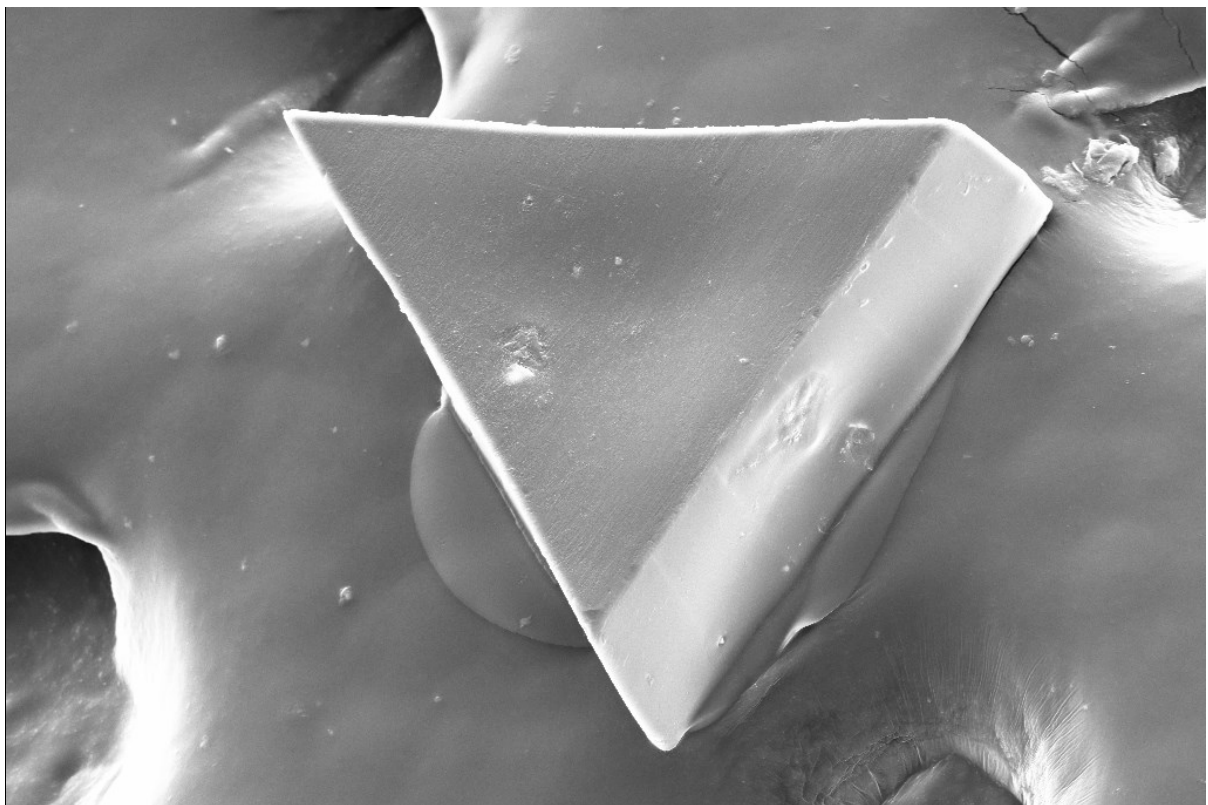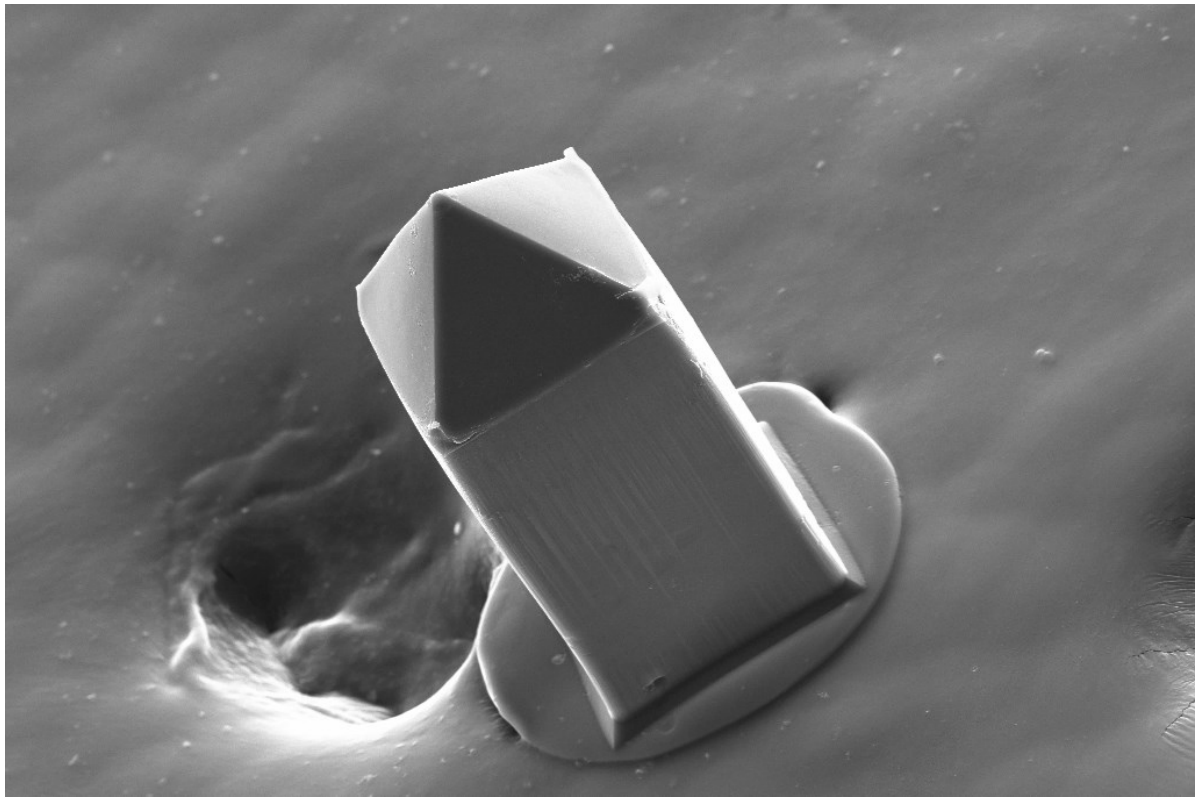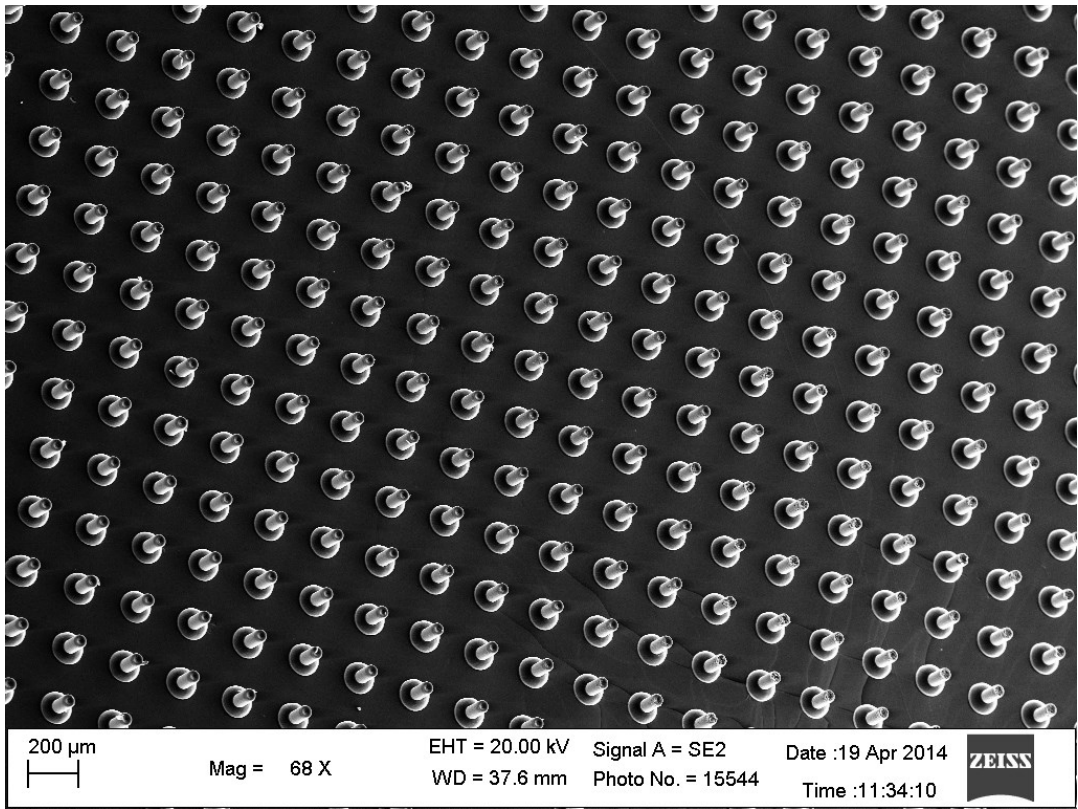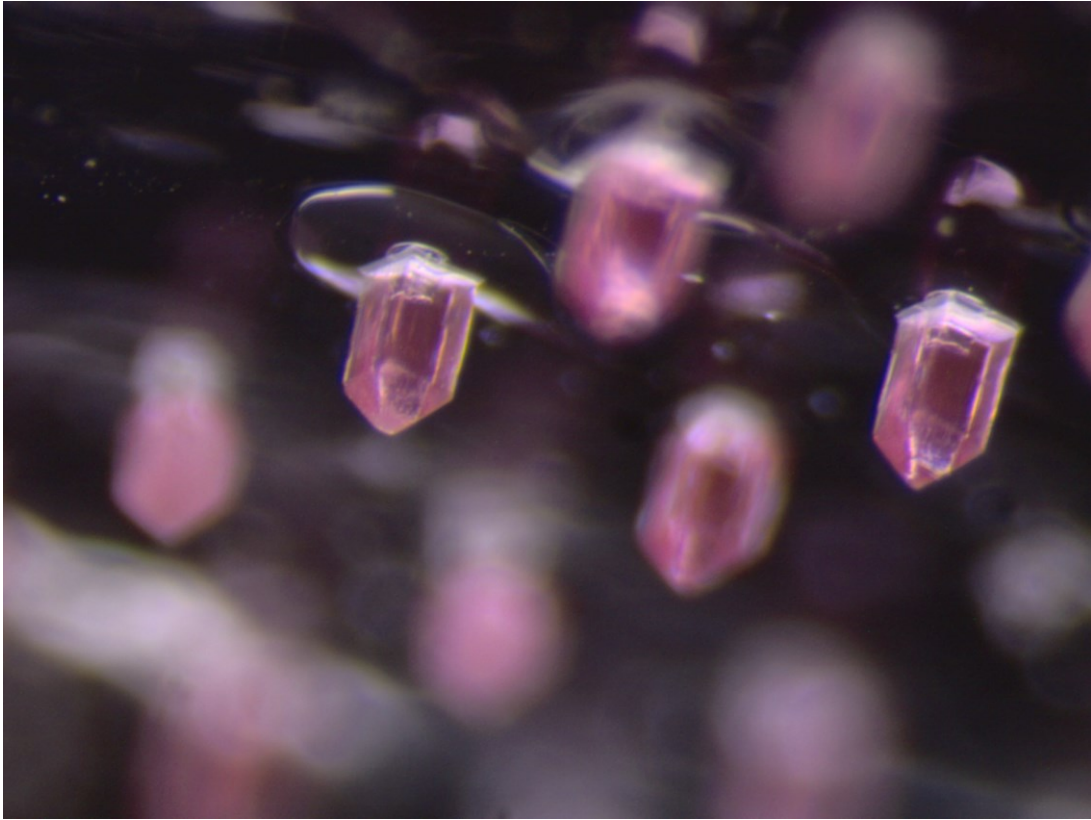
| 200 μm | Mag = 68 X | EHT = 20.00 kV | Signal A = SE2 | Date :19 Apr 2014 | ZEISS |
| WD = 37.6 mm | Photo No. = 15544 | Time :11:34:10 |

Mag = 1.23 K X · 20 µm · WD = 13.7 mm · EHT = 15.00 kV · Signal A = InLens · Date :6 Dec 2013 Time :11:46:53
ULTRA PLUS-43-04 · Noise Reduction = Pixel Avg. · ESB Grid = 492 V · System Vacuum = 2.98e-006 mbar

Mag = 861 X · 20 µm · WD = 25.0 mm · EHT = 5.00 kV · Signal A = SE2 · Date :8 Mar 2014 Time :9:37:57
ULTRA PLUS-43-04 · Noise Reduction = Pixel Avg. · ESB Grid = 492 V · System Vacuum = 2.85e-006 Torr